remote sensing

MDPI

Article

Identifying Precipitation and Reference Evapotranspiration Trends in West Africa to Support Drought Insurance

S. Lucille Blakeley [1,*,†], Stuart Sweeney [1], Gregory Husak [1], Laura Harrison [1], Chris Funk [2], Pete Peterson [1] and Daniel E. Osgood [3]

1 Department of Geography, University of California, Santa Barbara, CA 93106, USA; stuart.sweeney@ucsb.edu (S.S.); husak@geog.ucsb.edu (G.H.); harrison@geog.ucsb.edu (L.H.); pete@geog.ucsb.edu (P.P.)
2 U.S. Geological Survey, Earth Resources Observation and Science Center, 47914 252nd Street, Sioux Falls, SD 57198, USA; cfunk@usgs.gov
3 International Research Institute for Climate and Society, Columbia University, Palisades, NY 10964, USA; deo@iri.columbia.edu
* Correspondence: blakeley@ucsb.edu
† Current address: Department of Geography, University of California, Santa Barbara.

Received: 30 May 2020; Accepted: 27 July 2020; Published: 29 July 2020

Abstract: West Africa represents a wide gradient of climates, extending from tropical conditions along the Guinea Coast to the dry deserts of the south Sahara, and it has some of the lowest income, most vulnerable populations on the planet, which increases catastrophic impacts of low and high frequency climate variability. This paper investigates low and high frequency climate variability in West African monthly and seasonal precipitation and reference evapotranspiration from the early 1980s to 2016. We examine the impact of those trends and how they interact with payouts from index insurance products. Understanding low and high frequency variability in precipitation and reference evapotranspiration at these scales can provide insight into trends during periods critical to agricultural performance across the region. For index insurance, it is important to identify low-frequency variability, which can result in radical departures between designed/planned and actual insurance payouts, especially in the later part of a 30-year period, a common climate analysis period. We find that evaporative demand and precipitation are not perfect substitutes for monitoring crop deficits and that there may be space to use both for index insurance design. We also show that low yields—aligned with the need for insurance payouts—can be predicted using classification trees that include both precipitation and reference evapotranspiration.

Keywords: West Africa; climate variability; precipitation; evapotranspiration; index insurance

1. Introduction

Index insurance is an insurance product that pays out based on the performance of a weather indicator and is used to mitigate the impact of poor cropping seasons, often through targeting drought years [1]. This paper explores the efficacy of two weather indicators, precipitation and reference evapotranspiration, that are subject to decadal trends in West Africa. Our interest is in understanding how the choice of weather indicators may affect the robustness of index insurance programs. We document long-term trends in the indicators and explore how those trends cause a divergence between planned program payouts and expected program payouts. Using yield data as a direct measure of crop stress—the target of index insurance program intervention—we explore the degree to which the indicators are statistically associated with yields and can be used to predict the

lowest yield quantile. Our goal is to highlight potential issues in index insurance programs related to the choice of indicator and to inform as to how those issues might be mitigated.

1.1. Farming under Uncertainty

West African agriculturalists are primarily smallholder farmers dependent on rainfed cropping. They rely on a good rainy season to maintain their livelihoods [2] and often identify weather shocks as their greatest concern [3]. As a whole, West African farmers are at high risk of food insecurity [4]. Given their extreme poverty, they are ill-prepared to manage risks. Farmers respond to this through risk-averse behavior [5]. To ensure stable livelihoods, they employ risk-averting methods such as growing reliable crops (sorghum and millet), delaying planting until the rainy season has fully started, and forgoing investment in costly inputs like higher yield seeds or fertilizer [6]. However, farmers could attain more productivity through agricultural advancements by taking productive risks. Some agricultural practices for improved resilience include using genetically improved drought-resistant crop varieties [7,8], using fertilizer [9], or implementing water capture techniques such as contour ridges or demi lunes [10].

Agricultural advances can be complemented with financial tools to share risk and create risk reserves [11]. One financial tool is weather index insurance, which relies on a proxy measure of a hazard to identify payout events. Index insurance is similar to traditional insurance but pays out based on the poor performance of a weather indicator, unlike traditional insurance which pays out based on damages [12]. Index insurance is a risk management tool used to mitigate the impacts of a climate shock and is often used to mitigate the impacts of drought. Combined with other risk management strategies, index insurance can provide an additional safety net to help farmers experiencing poor growing conditions [13]. Risk-averse farmers can use index insurance to cover the uncertainty that any given year might be a bad year. Across the Sahel, where improved productivity is a necessity in the face of mounting climate variability and large population growth [14], index insurance has great potential to help millions of farmers. (Index insurance projects are ongoing across much of West Africa, targeting poor cropping years for different crops and using different indicators. These projects are functional and are already providing coverage for farmers in these areas. Our research goal is not to displace these projects but rather provide a guide for evaluating different indicators for index insurance. For further reference, these projects include but are not limited to the following: the World Food Programme's R4 index insurance project in Senegal [15], the World Bank and the Global Index Insurance Fund PlaNet Guarantee project in Benin, Burkina Faso, Mali, and Senegal [16,17], the African Risk Capacity index insurance project in the following West African countries: Burkina Faso, Mali, Niger, Senegal, and The Gambia, [18], and evapotranspirative projects through Environmental Analysis and Remote Sensing (EARS) in Senegal [19]).

1.2. Agroclimatic Indicators in West Africa

West Africa is classified as an arid region, with the rainy season defined as the West African Monsoon occurring from May to October [20]. The distribution of precipitation occurs through the intertropical convergence zone [21], and the majority of the precipitation in West Africa occurs from July to September [22], with August being the wettest month [23]. As seen in Figure 1a, West African precipitation has a sharp north-south gradient, where isohyets running east-west increase from north to south [24]. Similarly, the annual evaporative demand is characterized by east-west running isopleths of reference evapotranspiration (ET_0), seen in Figure 1b, which decrease from north to south [25]. Seasonal changes show high ET_0 to be related to high net radiation and temperature [25], indicating that when the sky is clear and the temperature is high, the evaporative demand is greatest.

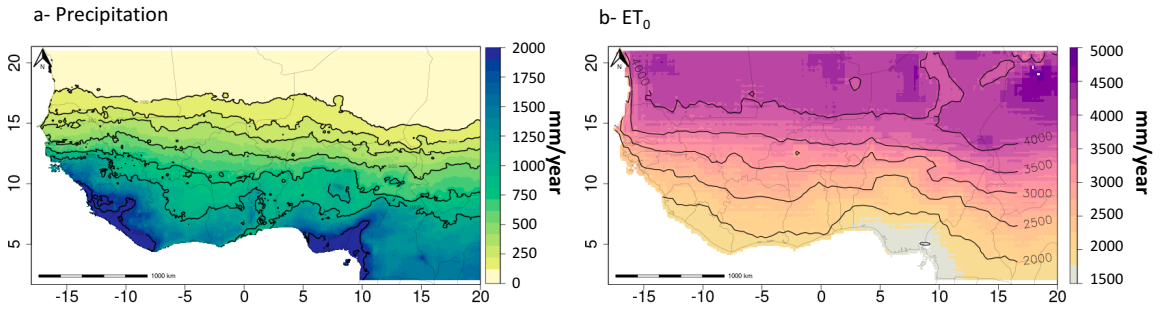

Figure 1. (**a**) Isohyets across West Africa, ranging from 100 mm/year in the far north of the Sahel to over 2000 mm/year in the south of West Africa (The amount of precipitation per year was capped at 2000 mm/year). Isohyets were calculated using yearly rainfall from the Climate Hazards InfraRed Precipitation with Stations dataset from 1981–2016 [26]. (**b**) Isopleths of ET_0 across West Africa, ranging from 5000 mm/year in the far north of the Sahel to under 1500 mm/year in the far south. (The amount of ET_0 was capped at 5000 mm/year). Isopleths of ET_0 used the ET_0 dataset produced by the National Oceanic and Atmospheric Administration's Physical Sciences Division from 1981 to 2016 [27,28].

West African precipitation exhibits a large amount of natural interannual and long-term variability, and predictability at seasonal scales is generally low [29]. Interannual variability is in part related to zonal winds where the African Easterly Jet is displaced farther north in anomalously wet years [23]. Long-term variability is related to sea surface temperatures fluctuating from the Atlantic Multidecadal Variability (AMV). The AMV drives 60% of the precipitation variability in the Sahel [30], which can result in decades with relatively high precipitation (abundant periods) or decades with low precipitation (drought periods).

Long-term climate change may also be influencing West African precipitation and evaporative demand. Biasutti and Sobel [31] found that for the 21st century simulation, an increase in simulated greenhouse gasses to the Coupled Model Intercomparison Project Phase Three (CMIP3) increased positive precipitation anomalies in October and negative precipitation anomalies in May/June. This delay in precipitation was also shown in CMIP5 simulations, where West Africa in particular experiences a delayed onset while across the Sahel there are stronger rains at the cessation of the rainy season [32].

ET_0 may be a useful proxy for identifying poor crop years. ET_0 measures the water needs of crops, estimating the amount of water that a hypothetical reference crop would evaporate and transpire in unlimited water conditions [33]. ET_0 was designed for irrigation management and has become an important agrometeorological parameter for climatological and hydrological analyses including drought identification [34,35].

Climate change is projected to increase temperatures in West Africa, which may contribute to ET_0 increases [36], resulting in higher risk of heat and water stress for agriculture [37,38]. The Intergovernmental Panel on Climate Change (IPCC) expects an overall increase in ET_0 in the Sahel during the 21st century [39]. However, Estes et al. [40] found large decreases in ET_0 during the rainy season in the Sahel. Cook et al. [20] found a more nuanced breakdown of the season, where ET_0 in West Africa increased during the early part of the season (May-June) but decreased in the later part of the rainy season.

1.3. Index Insurance in West Africa

Index insurance is designed to provide income to farmers during agroclimatic "bad" years as a partial substitute for lost farming income. In addition to direct income supplement effects, index insurance has been shown to have several positive indirect effects. Farmers with index insurance are more likely to invest in measures to increase production such as purchasing fertilizer [41]. In addition, banks may be more likely to provide credit to invest in productive inputs (expensive seed,

additional fertilizer) or even in irrigation systems [5]. These indirect effects can result in a significant increase in farmer production in an average year [13].

One class of index insurance protects against agroclimatic drought and is particularly well-suited to farming in West Africa, based on precipitation since often precipitation is the main determinant of a "good" yield [1]. These policies typically use precipitation deficits, for all or part of the season, to determine payouts. Determining the proper index and thresholds for payouts is a controversial and sensitive issue, as it needs to be straightforward for the policyholder but also complex enough to capture the variety of events that impact agricultural production. Although extremely high rainfall events can cause poor yields and adversely affect crops, they are difficult to accurately capture with remotely sensed data and therefore are not included in the scope of this research. Surveys, educational programs, and iterative tests have been done with farmers through organizations such as the World Food Programme to identify the appropriate indices to serve as proxies for the policies [41].

Index insurance targeting droughts use historical precipitation data, from an observation "window" spanning some or all of the rainy season, to calculate the threshold for payouts. If the precipitation falls below a certain amount, called a trigger, a partial payout occurs. A full payout occurs if the precipitation is below a different amount, called the exit. A critical aspect in the use of historical precipitation data is an understanding of low-frequency variability. In the last half-century, West African precipitation experienced low-frequency shifts from generally above-average precipitation in the 1950s to dry conditions of the 1980s and a recovery of rainfall during the 1990s until today [23]. If a positive precipitation trend is present, and insurance contracts ignore this trend, then these trends are likely to lead to the underpayment on index contracts held by farmers.

Because reliance on precipitation alone could be problematic, there is interest in using multiple independent datasets as inputs to the insurance index [42]. In a project funded by the International Fund for Agricultural Development [12], several data providers were asked to generate index insurance designs for drought-related farming losses in specific regions of Senegal. The seven service providers used a variety of remotely measured datasets: evapotranspiration, soil moisture estimates, satellite rainfall estimates, and Normalized Difference Vegetative Index (NDVI), a satellite measured vegetative product. They found that indices based on these datasets had similar accuracy in capturing drought, depending on the crop used for reference [12]. While use of multiple datasets may increase robustness of the resulting index, variability within datasets can affect index insurance products through changes in premiums, different identification of payout years, and the size of the payouts themselves.

1.4. Objectives

In this study, we focus on patterns of water supply (precipitation), atmospheric water demand (evapotranspiration, ET_0), and the implications of these spatial and temporal patterns on index insurance. We explore precipitation and ET_0 trends and indices during the period 1981–2016. This period is known to contain low-frequency variability moving from low precipitation in the 1980s to a rebound of precipitation in the late 1990s–2000s. We also investigate patterns in derived measures of agroclimatic drought such as the cessation of precipitation and the occurrence of dry spells during the rainy season. We then characterize the significance of these changes on index insurance and how insurance might combine these datasets to have more robust identification of poor agricultural conditions. Finally, we use yield data to better understand how these datasets might better serve applications such as index insurance.

2. Materials and Methods

We use data from three datasets (ET_0, precipitation, and one measure—Standardized Precipitation-Evapotranspiration Index, SPEI, derived from them) and observational crop data (yield). Trend analysis is used to identify the presence of low-frequency variability in each of the candidate measures. The results from the trend analysis are used to evaluate the impact of ignoring that variability

on insurance payouts and the degree of concurrence between candidate measures. Regression analysis is used to characterize association between the candidate measures and yield. Final regression and classification trees are used to predict lowest yield years (the target of index insurance) based on the full range of candidate measures.

2.1. Data

The precipitation data comes from the Climate Hazards Center InfraRed with Stations (CHIRPS) dataset (Downloadable at ftp://ftp.chc.ucsb.edu/pub/org/chg/products/CHIRPS-2.0/). CHIRPS blends a long-term climatology, satellite estimates of precipitation derived from cold-cloud duration calibrated to the Tropical Rainfall Measuring Mission (TRMM) dataset and available station observations [26]. Resolution for the CHIRPS dataset is 0.05° by 0.05°.

The ET_0 dataset (Downloadable at ftp://ftp2.psl.noaa.gov/Projects/EDDI/global_archive/. Documentation on this dataset available at https://psl.noaa.gov/eddi/globalrefet/) is produced by the National Oceanic and Atmospheric Administration's Physical Sciences Division (NOAA-PSD) global Evaporative Demand Drought Index (EDDI) [27,27,28,43,44] and was calculated with the American Society for Civil Engineers Penman-Monteith formulation [45]. The data is natively available at coarse-scale (0.5° × 0.625°) resolution and is subsequently resampled to fine-scale resolution (0.125° × 0.125°) by superimposing a 4 × 5 block grid using climatological estimates of monthly potential evapotranspiration from the the International Water Management Institute (IWMI). ET_0 calculations were done on a daily basis using daily means of 2-m air temperature, downward shortwave radiation at the surface, 2-m specific humidity, and 2-m wind speed from Modern-Era Retrospective Analysis for Research and Applications, Version 2, (MERRA-2) Reanalysis data [46]. ET_0 estimations are for a 0.12-m short grass reference crop. The ET_0 data is 0.125° by 0.125° resolution. To match the ET_0 and precipitation grids in certain analyses, the precipitation data were averaged per-pixel and resampled using nearest-neighbor to a 0.125° by 0.125° resolution.

A Standardized Precipitation and Evapotranspiration Index (SPEI) [47] was constructed by the authors from the CHIRPS precipitation dataset and the ET_0 dataset following the method as described by Vincente-Serrano et al. [48] using a log-logistic distribution for the period 1996–2016. SPEI is designed to capture droughts and supposedly reflect water balance in the target area by combining the hydrologic input to the system (precipitation) and removal of moisture from the system (evapotranspiration). Such an index should be able to account for poor cropping years, such as a year with high precipitation coupled with elevated ET_0.

Finally, a yield dataset (This data was collected and reported separately by the Ministry of Agriculture, Official Agricultural Statistics, Burkina Faso; Direction Nationale de l'Agriculture, Malie; Ministère de l'Agriculture, Niger; and Ministère de l'Agriculture et du Développement Rural, DAPSA, Senegal. Additional data cleaning was conducted internally, and the authors are responsible for the current data. This dataset can be shared, but requests to share are subject to review) was used in assessing the precipitation and ET_0 datasets for index insurance. This research combined sorghum and millet yield (defined as tonnes per crop produced per hectare, tonnes/ha), to have a sorghum-millet hybrid variable, hereafter referred to as yield. Twenty regions across the Sahel were chosen in Burkina Faso, Niger, Mali, and Senegal. Although these regions are relatively small in size, they are still larger than the pixel size of either the ET_0 or the precipitation data. Both of these datasets took the spatial average to match the region size. For drought insurance, large areas are impacted such that finer spatial resolution would not necessarily add more information to mesoscale droughts [49]. The yield data have 20 years' worth of yield data, from 1996 to 2016.

2.2. Trend Analysis

Precipitation, ET_0, SPEI, and index insurance indices were analyzed during the time 1981–2016 through trend analysis. Linear fit was used to estimate changes over time for June–October monthly totals of precipitation, monthly totals of daily means for ET_0, and seasonal totals for both. The months

were chosen based on the months that received the majority of the precipitation (July-September) and one month before and after the majority of the rainy season (June and October) to capture the ramp up and down of the rainy season. ET_0 data was regressed on precipitation to assess their linear relationship, using ET_0 as the response variable and precipitation as the independent variable.

To investigate the end of the rainy season and the distribution of the rains, two measures were developed with precipitation: the cessation of the season and number of dry pentads (5-day periods) per season. The cessation of the season is the period during which the season may end and is calculated as the first dekad (10-day period) with less than 5 mm of precipitation, followed by two dekads with a combined total of less than 10 mm of precipitation, using the dates 11 August through 31 December. The start and end date for calculating the end of the season were chosen to better target bad years, which may have a much earlier end of season. The last months of the year were picked to capture end of season in the Gulf of Guinea, which has a longer rainy season. Then, the number of dry pentads per season is calculated by adding the number of dry pentads with less than 5 mm from 1 June through the previously calculated cessation of season. Linear fit was then used to analyze trends for cessation of season and dry pentads.

2.3. Index Design

Insurance indices were made for both ET_0 and precipitation using the 15th percentile to approximate a 1 in 7 drought event (1/7 is approximately 14.3%) and used the 1981–2016 data, for the months of June–October and the seasonal totals. Any rate can be used to generate payouts for index insurance and in experiments testing farmers' interest in index insurance, the rates often range from 33% to 20% [50]. We chose the 15th percentile to target low probability poor precipitation events. Events more extreme than the empirically identified lowest (highest) 15th percentile for precipitation (ET_0) threshold were considered a "bad" year and would require a payout. In this index the "payout" is binary, each year being identified as a payout year or not, with no exploration of fractional payouts for this test. Although indices typically have a sliding scale, since this paper is focusing on different datasets for index insurance purposes, and not on the payouts themselves, our choice of binary payouts is appropriate.

2.4. Heidke Skill Score

The Heidke Skill Score was used to measure agreement between the precipitation payouts and the ET_0 payouts, both seasonally and for the months June–October. The Heidke Skill Score measures the skill of predictions using hits, correct negatives, misses, and incorrectly predicted hits [51]. This analysis considers "hits" as years where both ET_0 and precipitation have payouts, "correct negatives" are years where neither ET_0 nor precipitation had a payout, and misses or incorrectly predicted hits are where the payout years disagree between datasets. The results of the Heidke Skill Score were translated into total number of agreeing payout years, ranging between 0 (locations that never had a payout match between precipitation and ET_0) and 5 (all possible payouts matched). A comparison of the first and second half of the payouts was conducted, where the payout data was split into 1981–1998 and 1999–2016.

2.5. Linear Regression

Association between the environmental indicators (precipitation, ET_0, and SPEI) and yield can be empirically assessed using regression analysis. We use regional yield and the associated environmental measures for the same region and growing season. The yield data is first examined via linear fit with seasonal totals of precipitation, ET_0, and SPEI. The empirical bivariate relationships were assessed using pooled data over the full set of the locations in the region. Using a pooled model increases the power to find statistically significant relationships if some of the β coefficients can be held fixed.

Specification testing, outlined in the Appendix A, indicates that Equation (1), which has a fixed slope and varying intercept is the best equation for capturing yield.

$$y_{i,t} = \alpha_i + \beta_1 X_{i,t} + u_{i,t} \quad (1)$$

where $y_{i,t}$ is the regional (i) and year (t) indexed yield, and $X_{i,t}$ is either precipitation, ET_0, or SPEI. Note that α_i models the unobservable time-invariant regional effect.

2.6. Classification and Regression Tree Analysis

While statistically significant association is of interest as a check whether the measures reflect the underlying biological relationship linking environmental growing conditions to crop outcomes, this metric does not directly address whether the indicators can predict crop failures. Classification and Regression Trees (CART) can be used to predict low yields using a set of partially collinear environmental indicators (SPEI, ET_0, and precipitation) as well as country indicators (to allow for regional heterogeneity). In CART, the algorithm searches over the range of each candidate regressor independently to identify the split that provides the best predictive accuracy. All regressors are considered as candidate criteria by which to split the data, until a stopping rule is reached. In classification tree analysis the outcome is binary, which in our models takes the value 1 if yield is in the lowest 20% and 0 otherwise. Regression tree analysis is an alternative formulation to classification trees, where the data is not binary but rather continuous. The splitting criteria in regression tree analysis tries to most efficiently partition the data into as homogeneous as possible yield regimes.

3. Results

3.1. Precipitation

Some broad spatial patterns become apparent from the maps in Figure 2. Precipitation overall has a generally positive trend for individual months across large swaths of the Sahel during the 36 years of analysis. First, Figure 2c,d show that north of 14° N there is a positive precipitation trend in August and September, and central West Africa experiences a slight increase in precipitation in June (Figure 2a) and July (Figure 2b). During October, the 7° N latitude has shown a positive precipitation trend along the Coast of Guinea. Additionally, the overall change for June–October season (Figure 2f) shows a positive increase in precipitation across the 13–15° N latitude.

The trends in the cessation of the season and dry pentads point to the rainy season overall changing in structure. In Figure 3a, the trend for the cessation of the season is positive in central West Africa, particularly around 12° N to 16° N from 15° W to 15° E, indicating that the rainy season is ending later here. There are additional spots, such as over 3° E to 4° E from 6° N to 10° N and from 10° W to 15° E above the 15° N latitude that have a later end of season overall. The locations where overall there is no change in the later end of season is south of 10° N from 15° W to 2° W and 5° E to 20° E. Results show an overall change of around 0.5 days/year. Across the 36 years used for this study, that would indicate a delay in the cessation of season by 16 days (approximately half a month). The locations where overall there is no change in the later end of season are south of 10° N from 15° W to 2° W and 5° E to 20° E. Additionally, in Figure 3b, the trend for the total number of dry pentads is negative, indicating there is a general decrease in the number of dry pentads over time. The trend for the start of season was also calculated but was not significant.

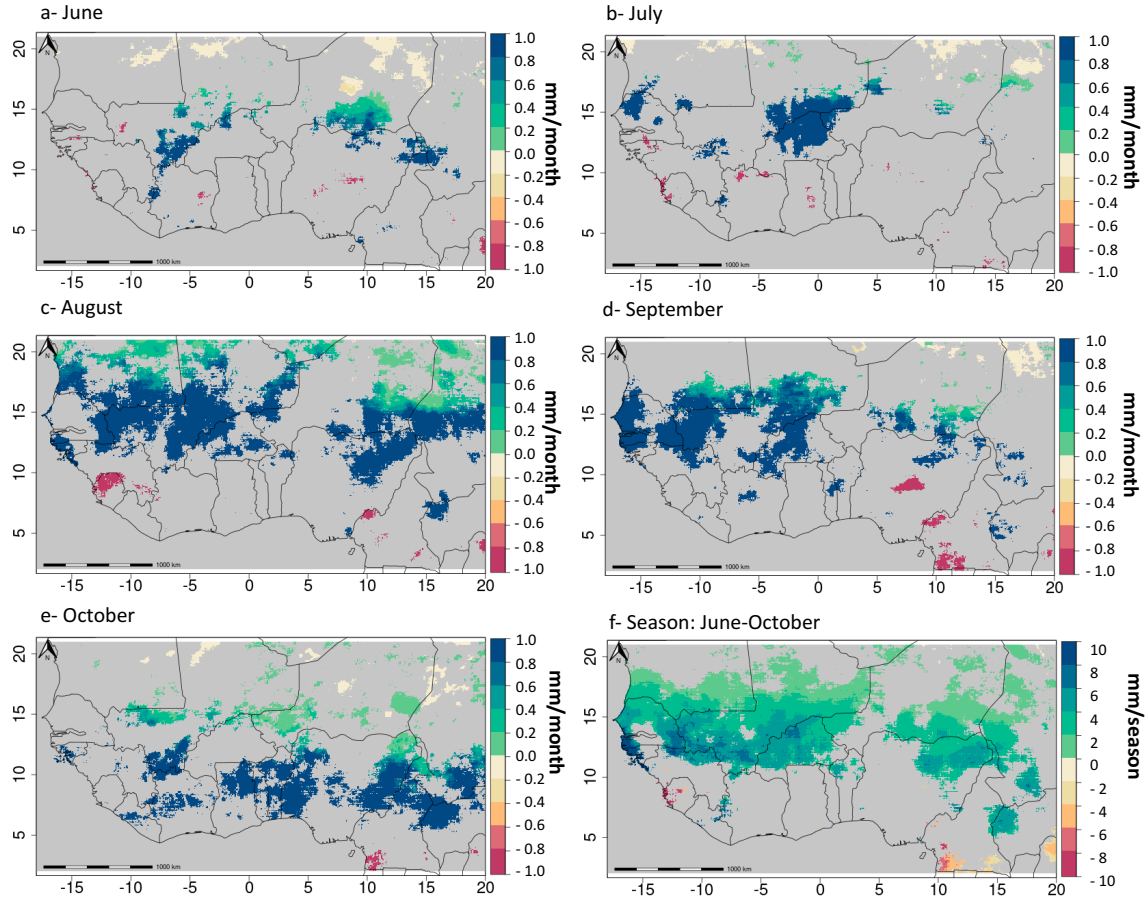

Figure 2. Precipitation regressions for the months of June (**a**), July (**b**), August (**c**), September (**d**), October (**e**), and full season (**f**) from 1981 to 2016, in mm/month for (**a**) through (**e**), and in mm/season for (**f**). The data in (**a**–**e**) is capped at −1 to 1 mm, and the data in (**f**) is capped at −10 to 10 mm. Any insignificant trend ($p > 0.05$) has been masked out in gray.

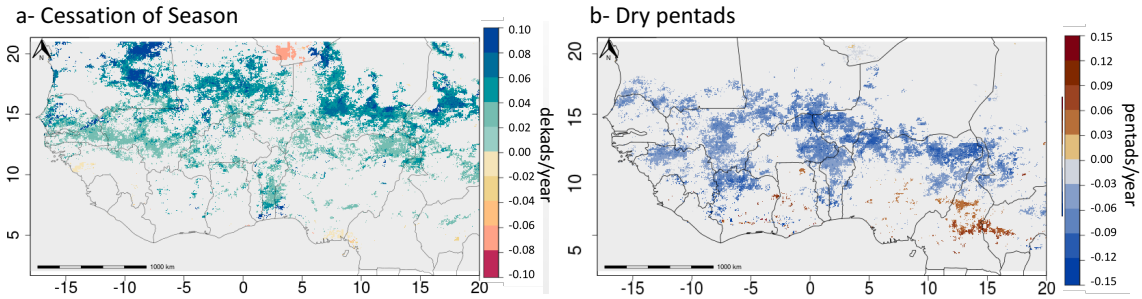

Figure 3. (**a**) Trend for the cessation of the season, as measured by dekads per year, calculated from 1981 to 2016. Capped at −0.1 to 0.1 dekad/year, insignificance ($p > 0.05$) is masked out in gray. (**b**) The trend of total number of dry pentads for the season, as measured in pentads/year, calculated from 1981 to 2016. Capped at −0.15 to 0.15 pentads/year, insignificance ($p > 0.05$) is masked out in gray.

3.2. ET_0

The patterns observed in the ET_0 trends vary throughout the summer months, and, unlike precipitation, a general regional trend is not readily apparent. As seen in Figure 4, ET_0 trends depend on the month and location. East of 10° E and west of 7° W show increases in evaporative

demand in all the months, varying in spatial extent. From 5° W to 5° E there is decreasing ET_0 during June (Figure 4a), September (Figure 4d), and October (Figure 4e). In August (Figure 4c) there is a broad decreasing band in evaporative demand extending from 13° N to 20° N and between 15° W to 15° E. This prominent feature from the August (Figure 4c) map is much less pronounced in September (Figure 4d) and October (Figure 4e). The coast from 14° W to 15° W along the 11° N to 15° N has decreasing ET_0 in all months. For the whole season (Figure 4f), there is an decrease along the 15–13° W from 11–20° N, particularly in the July (Figure 4b), September (Figure 4d), and October (Figure 4e) months, with a marked increase from 10 to 20° E from 0 to 5° N, a feature that is present in all months except September.

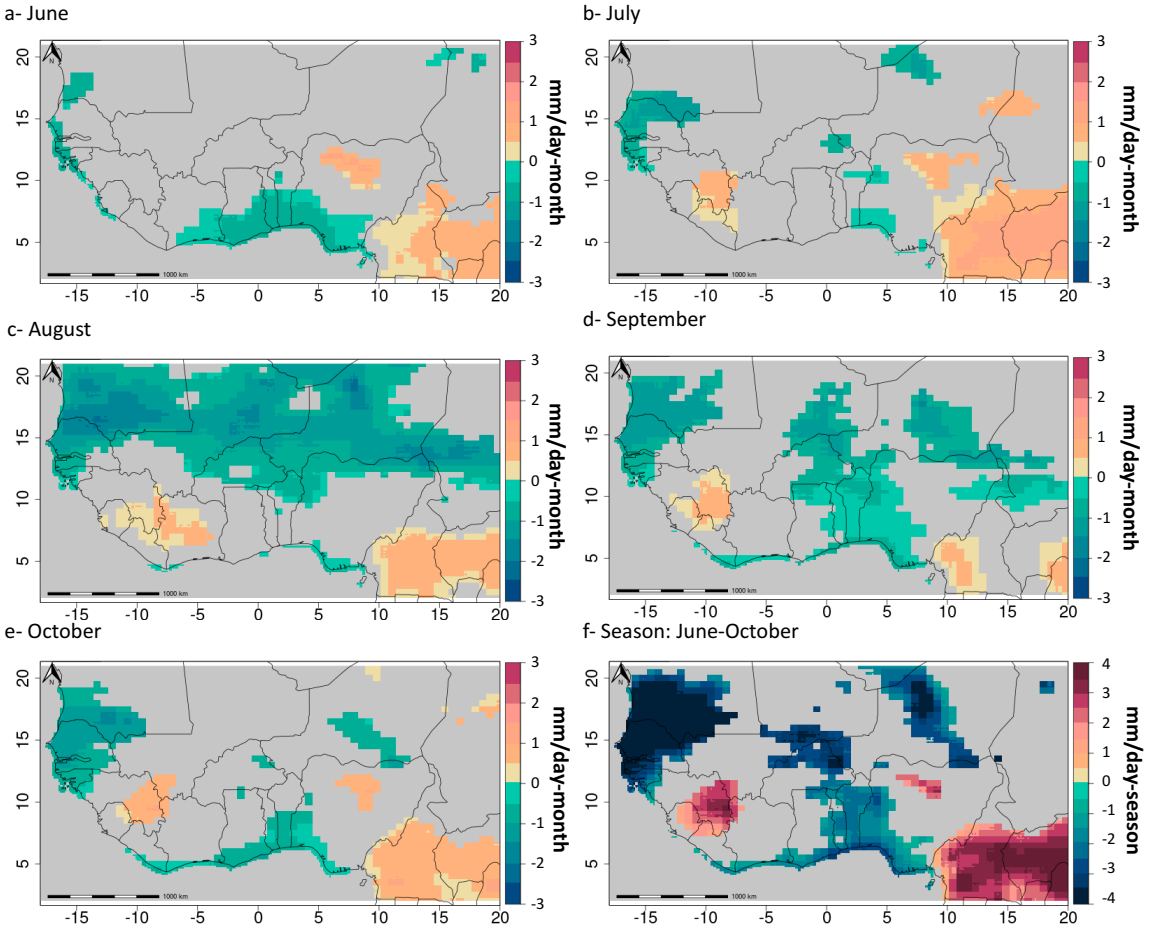

Figure 4. ET_0 regressions for the months of June (**a**), July (**b**), August (**c**), September (**d**), October (**e**), and full season (**f**) calculated from 1981 to 2016. The units in (**a**) through (**e**) have been capped to −3 to 3 mm day^{-1} month^{-1}, while the units in **f** have been capped from −4 to 4 mm day^{-1} season^{-1}. Any insignificant slope ($p > 0.05$) has been masked out in gray.

3.3. ET_0 and Precipitation

This relationship is shown in Figure 5, where the correlation between precipitation and ET_0 is largely negative, particularly during August, September, and October along 14° N to 15° N. From the coast to the north across 4° W to 4° E for July, August, and October, the slopes are also negative. For the overall season, see in Figure 5f, there is a strong negative correlation between precipitation and ET_0, particularly across the 15–18° N latitude. This negative relationship is expected, as the rainy season presents more cloud cover, resulting in lower solar radiation and ultimately decreasing ET_0. Unsurprisingly, the relationship in the Sahara (approximately 15° N and northward) exhibits a strong negative relationship throughout the season between ET_0 and precipitation, which is particularly

prominent in August, September, and the overall season. In general, drier areas exhibit a stronger inverse relationship.

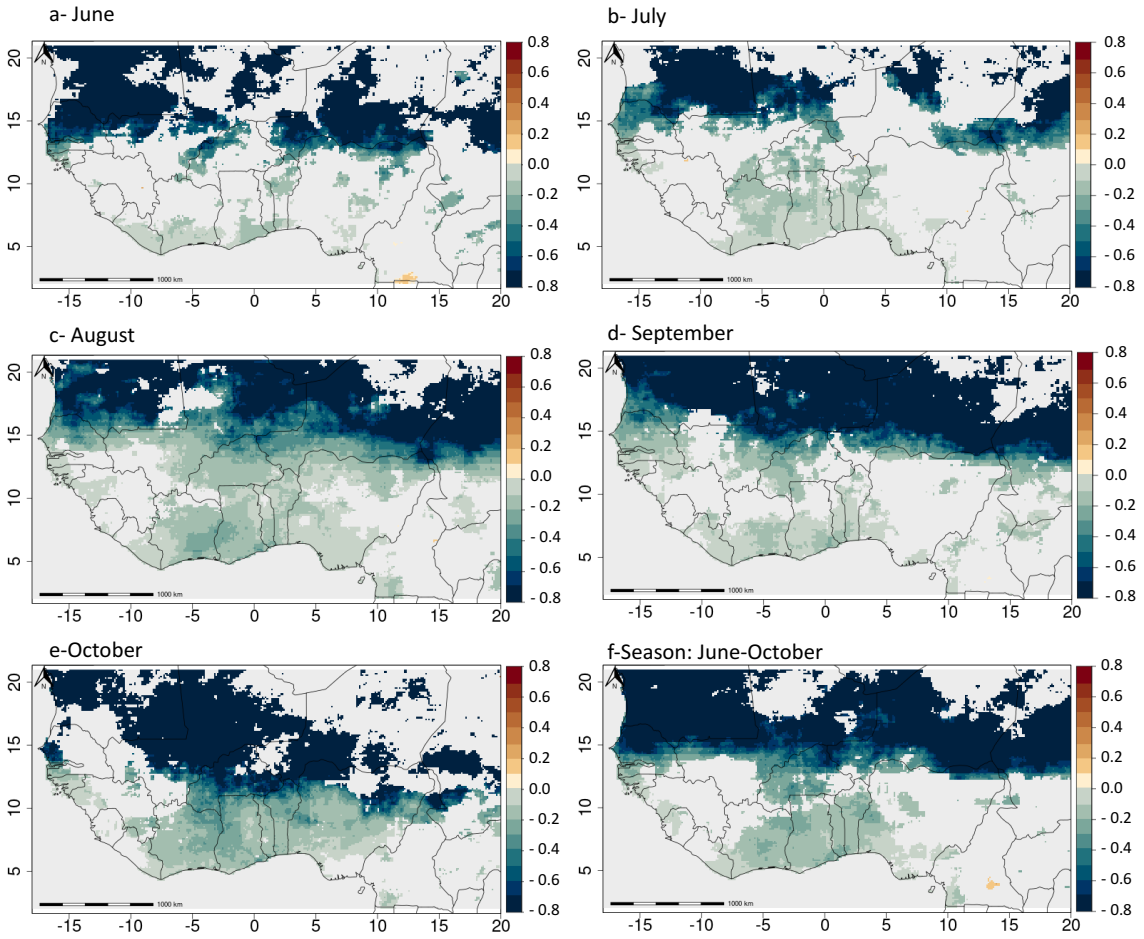

Figure 5. ET_0 regressed on precipitation, where precipitation is the independent variable and ET_0 is the dependent variable for the months of June (**a**), July (**b**), August (**c**), September (**d**), October (**e**), and full season (**f**) calculated from 1981 to 2016. Any insignificant slope ($p > 0.05$) has been masked out in gray.

3.4. Indices and Heidke Skill Score

The precipitation index and ET_0 index pay out at different critical times. The payout rate of once every seven years (1/7) resulted in 5 payouts over the 1981–2016 time series. The monthly payouts for precipitation and ET_0 are shown in Figure 6, along with the corresponding Heidke Skill Score for each month. In the precipitation index, there are generally a low number of payouts in the years 1999–2016, although there are exceptions in the northern-most and southern-most parts of West Africa, where some locations have a higher rate (4–5) of payouts during the latter half of the record. During July–October, many locations in central West Africa, along the 13–15° N latitude experience 0–2 payouts. For the ET_0 index, payouts have a greater range than precipitation payouts from 1999 to 2016. August, for example, receives fewer payouts while June and October receive more payouts during this time.

The agreement between the precipitation and ET_0 payouts varies by month, as analyzed in the Heidke Skill Score in Figure 6k–o. The monthly index Heidke Skill Scores in Figure 6k–o range from no agreement to strongly agree, and the seasonal indices have more agreement than the monthly payouts except August. June and July are the months that overall have the lowest agreement, with September agreement being only slightly higher. August has the highest overall agreement, with agreement

throughout central West Africa and western West Africa. There is additionally high agreement in the southern part of West Africa during October. Considering that there is a significant negative relationship between ET_0 and precipitation for August (Figure 5c), the high Heidke Skill Score for this month is unsurprising. The agreement for the seasonal indices is better than all months except August. In particular, in Figure 7a, the precipitation index has less than 2 payouts overall for 1999–2016 across the 13–15° N latitude. In contrast, the ET_0 index experiences between 2 and 5 payouts for the same 13–15° N latitude region.

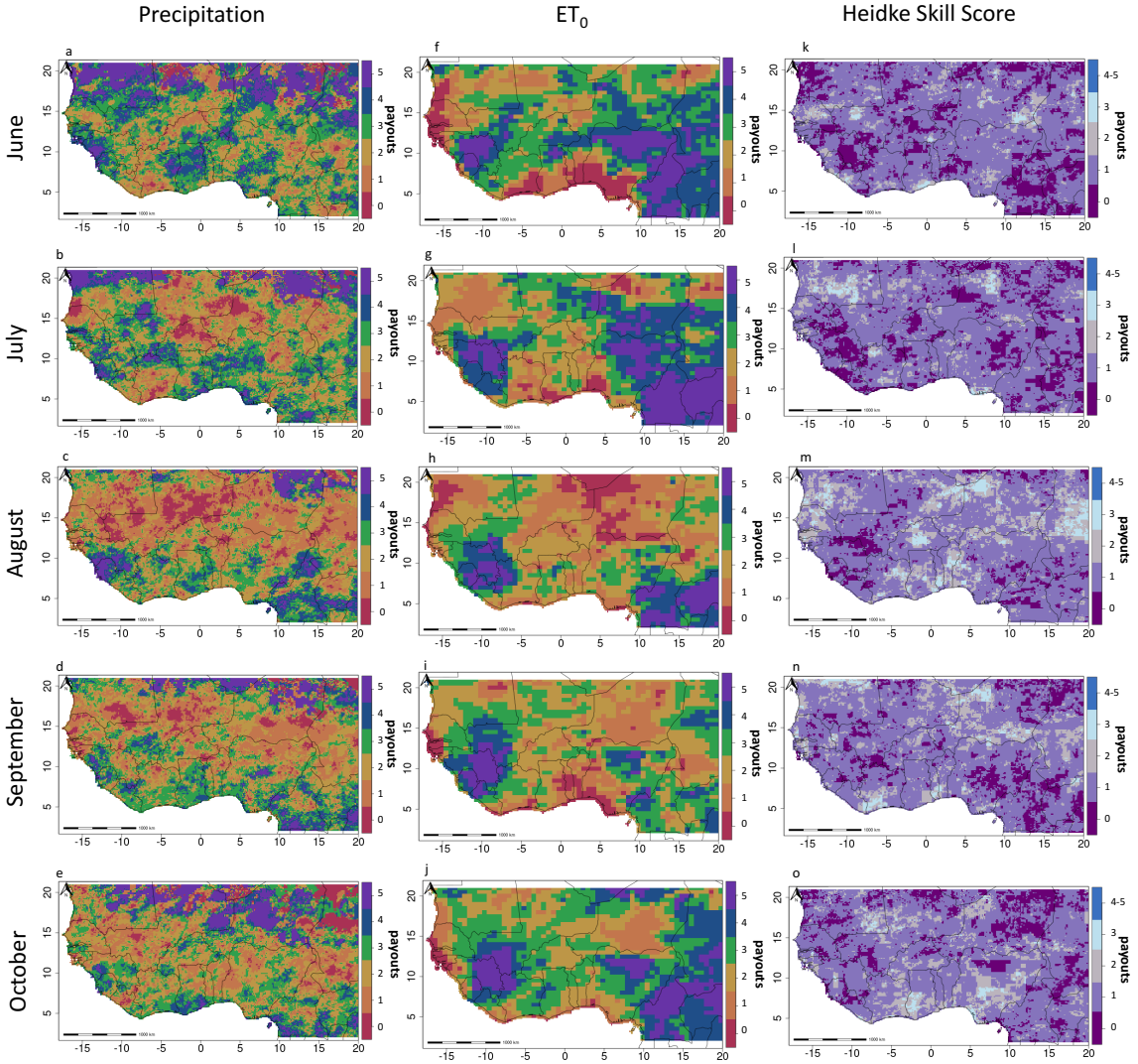

Figure 6. (**a**–**e**) (Left, Top to Bottom) June (**a**), July (**b**), August (**c**), September (**d**), October (**e**) payouts that occurred for 1999–2016 precipitation data. (**f**–**j**) (Middle, Top to Bottom) June (**f**), July (**g**), August (**h**), September (**i**), October (**j**) payouts that occurred for 1999–2016 ET_0 data. (**k**–**o**), (Right, Top to Bottom) June (**k**), July (**l**), August (**m**), September (**n**), October (**o**), Heidke Skill Score for the payouts of ET_0 to the precipitation payouts. These plots show where the precipitation data and the ET_0 data have between 0 and 5 payouts occurring in the same year. To match the ET_0 and precipitation grids, the precipitation data were averaged per-pixel and resampled using nearest-neighbor. However, although some areas in the ET_0 appear more coarsely mapped than the precipitation data or the Heidke Skill Score maps, this appearance is a known consequence of the method in https://psl.noaa.gov/eddi/globalrefet/ used to downscale the ET_0 spatial resolution from 0.5° × 0.625° resolution to 0.125° to 0.125° × 0.125° resolution and is not an artifact in our analysis in this study.

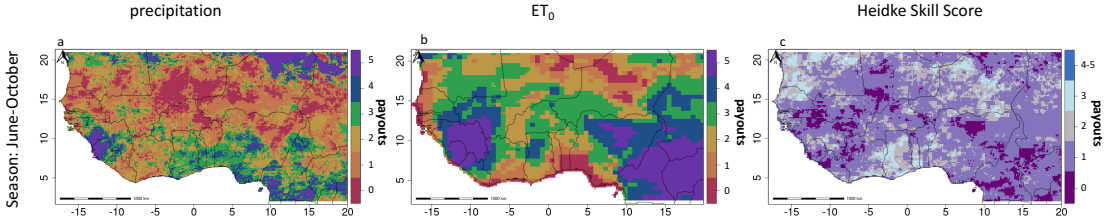

Figure 7. (**a**) Seasonal payouts that occurred during 1999–2016 in the precipitation dataset. (**b**) Seasonal payouts that occurred during 1999–2016 in the ET_0 dataset. (**c**) Heidke Skill Score for the payouts of ET_0 to the precipitation payouts. This plot shows where the precipitation data and the ET_0 data have between 0 and 5 payouts occurring in the same year.

3.5. Linear Fits with Yield, Precipitation, ET_0, and Spei

Coefficient estimates, standard errors, and other diagnostics for model (1) using either precipitation, ET_0, or SPEI as the independent variable are provided in Table 1. The model results in Table 1 show that the independent variables (precipitation, ET_0, and SPEI) all have significance in predicting yield and have correspondingly high R-squared. It is clear that precipitation, ET_0, and SPEI capture variation in the yield reasonably well. All three of these variables are significant at the p-value < 0.001 level. The relationship is present in all regions, with each region having a modifying variable for the region. Additionally, all models have a relatively high adjusted R-squared, with precipitation's R-squared at 0.6649, ET_0's R-squared 0.6784, and SPEI's R-squared at 0.6692 (see Figure 8a–c).

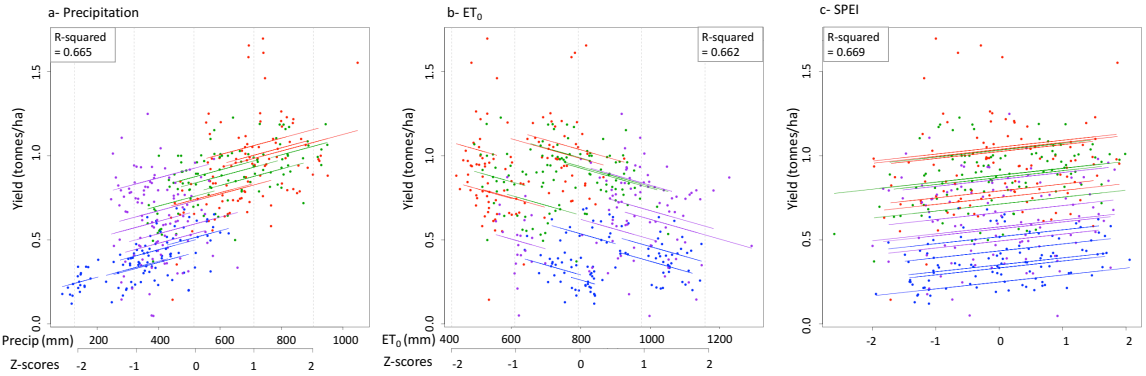

Figure 8. Using yield data, precipitation, ET_0, and SPEI for 1996–2016, (**a**) this image shows the regression of precipitation predicting yield. (**b**) this image shows the regression of ET_0 predicting yield. (**c**) this image shows the regression of SPEI predicting yield. The data are identified by country in different colors: Burkina Faso represented in red, Mali in green, Niger in blue, and Senegal in purple. There were five regions per country, which are further represented by different regression lines in the plots—all plotted with corresponding colors to the country they are in. Further information on specifications of the regression models can be found in Table 1.

Table 1. Regressions Predicting Yield Numbers within the brackets () represent the standard error of the estimate directly above themselves. Different *p*-values are used to determine significance—* represents estimates that *p*-values smaller than 0.05, ** represent estimates that have *p*-values smaller than 0.01, and *** represent estimates that have *p*-values smaller than 0.001.

	Model 1: Precipitation	**Model 2: ET_0**	**Model 3: SPEI**
Intercept	0.4954 ***	1.1026 ***	0.7521 ***
	(−0.0759)	(−0.1039)	(−0.0379)
X_1	0.0005 ***	−0.0006 ***	0.2856 ***
	(−0.0001)	(−0.0002)	(−0.0536)
Burkina-Kenedougou	0.1494 *	0.2278 ***	0.0385 ***
	(−0.0634)	(− 0.0564)	(−0.0535)
Burkina-Kouritenga	−0.0085	−0.0046	0.0385
	(−0.0551)	(0.0554)	(−0.0535)
Burkina-Mouhoun	0.226 ***	0.402 ***	0.2988 ***
	(−0.0568)	(0.0611)	(−0.0535)
Burkina-Silassi	0.1684 **	0.3503 ***	0.2726 ***
	(−0.0596)	(−0.0611)	(−0.0535)
Mali-Kayes	0.0436	0.0946	0.1179 *
	(−0.057)	(−0.0544)	(−0.0535)
Mali-Koulikoro	0.0972	0.2928 ***	0.1325 *
	(−0.0546)	(−0.0699)	(−0.0535)
Mali-Mopti	0.0191	0.0131	−0.0396
	(−0.0557)	(−0.056)	(−0.0535)
Mali-Segou	0.1347 *	0.3019 ***	0.1315 *
	(−0.0539)	(−0.0716)	(−0.0535)
Mali-Sikasso	0.1265	0.3539 ***	0.2808 ***
	(−0.066)	(−0.0587)	(−0.0542)
Niger-Bouza	−0.2407 ***	−0.0557	−0.3178
	(−0.0571)	(−0.0902)	(−0.0535)
Niger-Dosso	−0.2264 ***	−0.0975	−0.2338 ***
	(−0.05459)	(−0.0665)	(−0.0542)
Niger-Filingue	−0.3094 ***	−0.3415 ***	−0.4191 ***
	(−0.0602)	(−0.0582)	(−0.0535)
Niger-Goure	−0.3062 ***	−0.3722 ***	−0.5024 ***
	(−0.073)	(−0.0656)	(−0.0542)
Niger-Mayahi	−0.3162 ***	−0.1432	−0.4006 ***
	(−0.0582)	(−0.0891)	(−0.0542)
Senegal-Diourbel	−0.0719	0.1062	−0.1752 **
	(−0.0596)	(−0.0945)	(−0.0535)
Senegal-Fatick	−0.0092	0.1580	−0.09
	(−0.0574)	(−0.0871)	(−0.0535)
Senegal-Foundiougne	0.1864 **	0.3092 ***	0.1071 *
	(−0.0573)	(−0.0776)	(−0.0535)
Senegal-Gossas	−0.1458 **	−0.0115	−0.1868 ***
	(−0.0549)	(−0.0725)	(−0.0535)
Senegal-Mbacke	−0.2022 ***	−0.2458 ***	−0.2593 ***
	(−0.0557)	(−0.0542)	(−0.0535)
Adjusted R-squared	0.6649	0.6784	0.6692
F-statistic	42.16	41.65	42.97
Degrees of Freedom	395	395	395

3.6. Regression Tree Analysis of Crop Yield

The regression tree, seen in Figures 9–12, finds that for Niger, Burkina Faso, and Mali, the splits between precipitation accurately separate the yields into different high, medium, and low classes. For Niger, the single rule between 314.7 mm splits the observations into low yield (0.27 tonnes/ha). For Burkina Faso and Mali, the initial rule splits the observations into high yield (1.02 tonnes/ha) and

medium/lower yield. The second rule for Burkina Faso and Mali splits the observations to medium yield (0.85 tonnes/ha) when there is less precipitation than 680.2 mm but more precipitation than 460.6 mm and low yield (0.62) when there is less precipitation than 460.6 mm. The regression tree results for Senegal are more mixed. Surprisingly, the lowest yield (0.49 tonnes/ha) is when the ET_0 is less than 749.1 mm, which would be expected to have the highest yield since the evaporative demand is low. This may indicate issues related to poor crop yield data, as well as other factors than climate on yield (i.e., socio-economic influences, governmental influences, soil quality, etc). The second lowest yield (0.58 tonnes/ha) occurs when the ET_0 is greater than 997.5 mm, which would be more in line with the expectation for an association between yield and ET_0. When the ET_0 is between 749.1 mm and 997.5 mm, the final rule in the Senegalese observations is precipitation greater (less) than 367.4, which results in another surprising result—the high precipitation has a lower yield (0.67 tonnes/ha) amount than the lower precipitation yield (0.91 tonnes/ha).

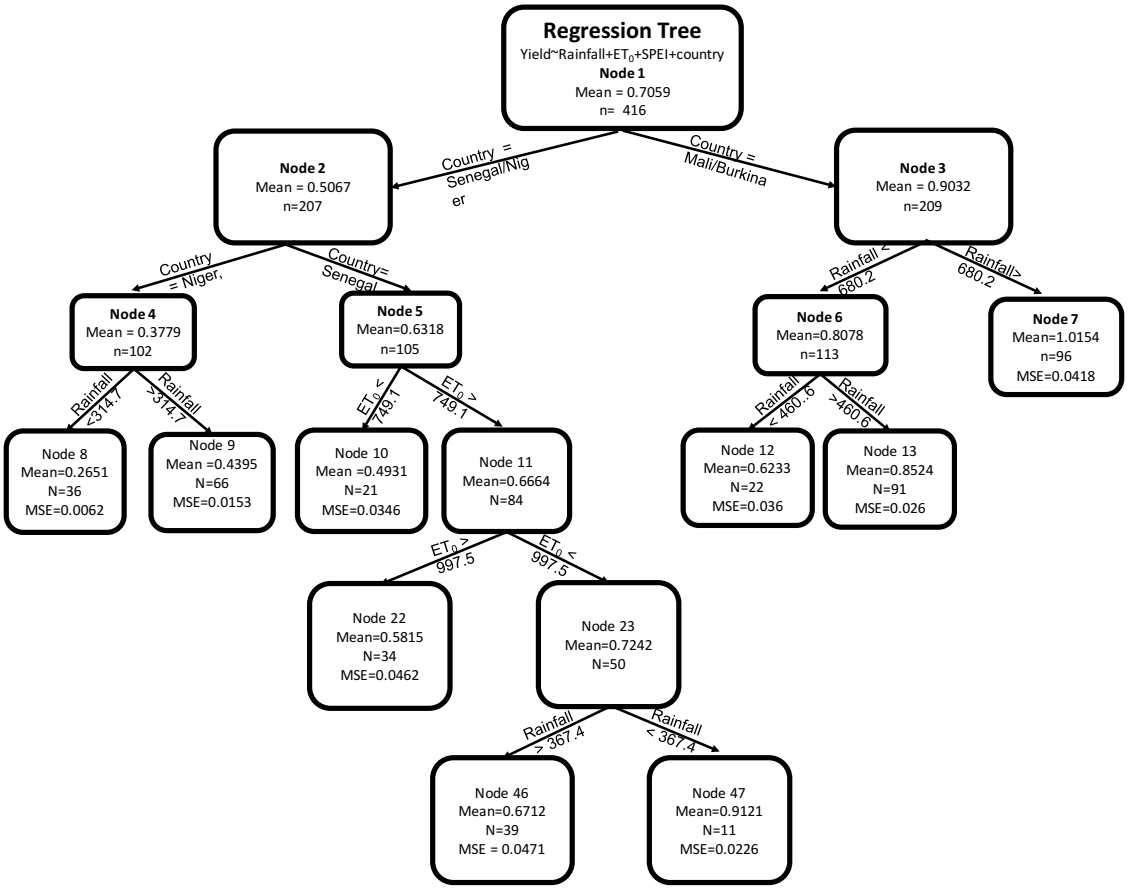

Figure 9. The regression tree for yield across all regions using seasonal precipitation, seasonal ET_0, and seasonal SPEI to classify the yield into classes. Seasonal SPEI was ultimately not used for splitting the data in this regression tree.

3.7. Classification Tree Analysis of Low Yield Years

Precipitation, ET_0, and SPEI are also used as the classification candidates to predict low yield years, defined as years that are lower than the 20th percentile of yield. Figure 13 provides a visual representation of the classification tree and a summary of the splitting criteria. Precipitation and ET_0 are selected in the model to predict poor growing years. The final classification tree has two rules, using first precipitation to split the observations into high precipitation (greater than 317.7 mm) and low precipitation (less than 317.7 mm). The second rule splits ET_0 into high evaporative demand (greater than 892.5 mm) and low evaporative demand (less than 892.5 mm). There is one node that has 100% crop failures, which has low precipitation and low evaporative demand. The node that has

low precipitation but high evaporative demand has a 66.7%/33.3% split between crop successes and failures. The node that splits the data into high precipitation has 88.4% of the observations being crop successes and 11.6% of the observations as crop failures.

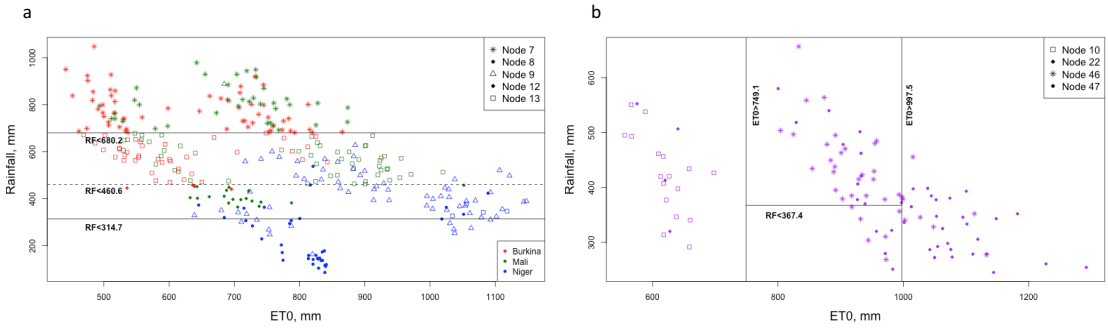

Figure 10. (**a**) The regression tree for Burkina Faso, Mali, and Niger plots ET_0 against precipitation. The rules for Burkina Faso and Mali have the first rule of precipitation greater (less) than 680.2 mm and the second rule of precipitation greater (less) than 460.6. The rule for Niger has precipitation greater (less) than 314.7 mm. (**b**) The regression tree for Senegal plots ET_0 against precipitation. The first rule is ET_0 greater (less) than 749.1 mm. The second rule is ET_0 greater (less) than 997.5 mm. The final rule is precipitation greater (less) than 367.4 mm.

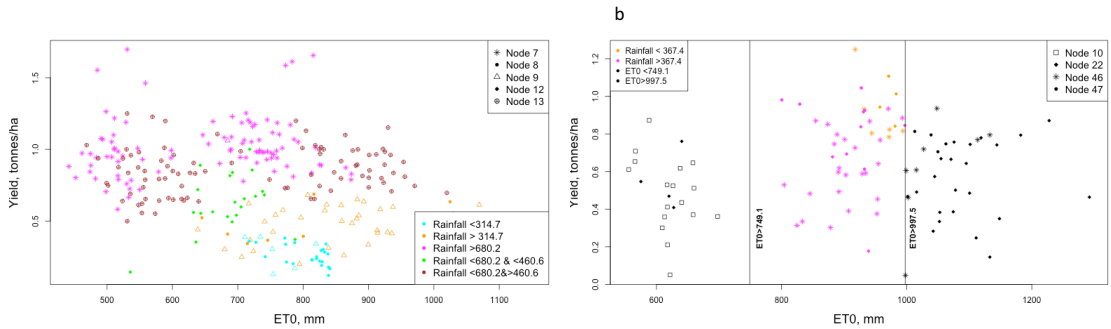

Figure 11. (**a**) The regression tree results for Burkina Faso, Mali, and Niger plotted with ET_0 against yield, with different dot shapes denoting which node in the regression tree the yield falls into. The dots are separated by different colors for the precipitation rules—for Burkina Faso and Mali, the precipitation greater than 680.2 mm is represented as pink, the precipitation between 680.2 mm and 460.6 mm is represented as dark red, and precipitation less than 460.6 is represented as green. For Niger, the precipitation greater than 314.7 mm is represented with blue, and the precipitation less than 314.7 is represented as orange. (**b**) The regression tree results for Senegal, plotting ET_0 against yield, with different dot shapes representing which node in the regression tree the yield falls into. The dots are separated by different colors for the precipitation rules, and there are lines representing the ET_0 rules. The first rule is ET_0 greater (less) than 749.1 mm, and the second rule is ET_0 greater (less) than 997.5 mm. The next rule is precipitation greater than 367.4 mm (represented by pink) and precipitation less than 367.4 mm (represented by orange).

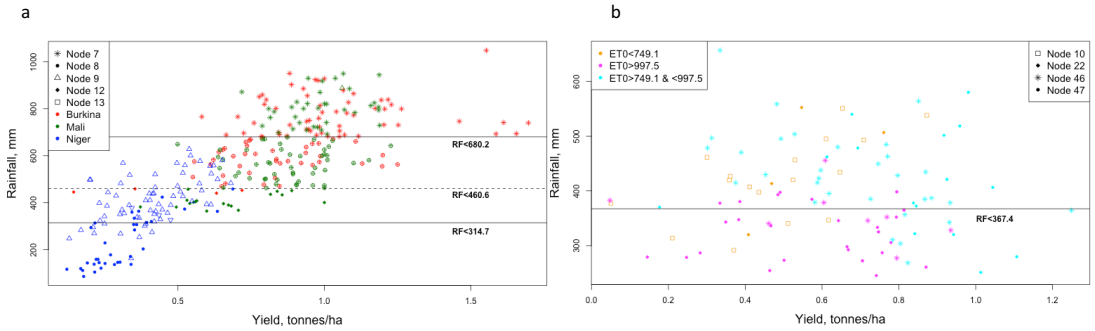

Figure 12. (**a**) The regression tree results for Burkina Faso, Mali, and Niger with yield plotted against precipitation; the different dot shapes represent the nodes the observation is under and the different dot colors represent the country the observation is from, with lines representing the regression tree rules for precipitation. The first rule for Burkina Faso and Mali data is precipitation greater (less) than 680.6 mm, and the second rule is precipitation greater (less) than 460.2 mm. The rule for Niger observations is precipitation greater (less) than 314.7 mm. (**b**) The regression tree results for Senegal with yield plotted against precipitation, the different dot shapes representing the node the observation is under and the different dot color representing the ET_0 rules, with a line representing the rule for precipitation. The first rule splits data into greater than 749.1 mm and less than 749.1 mm (represented in orange). The second rule splits data into greater (less) than 997.5 mm, with data that is greater than 997.5 represented in pink. The data that falls between 997.5 mm of ET_0 and 749.1 mm are represented in blue, and are subject to the precipitation rule of greater (less) than 367.4 mm.

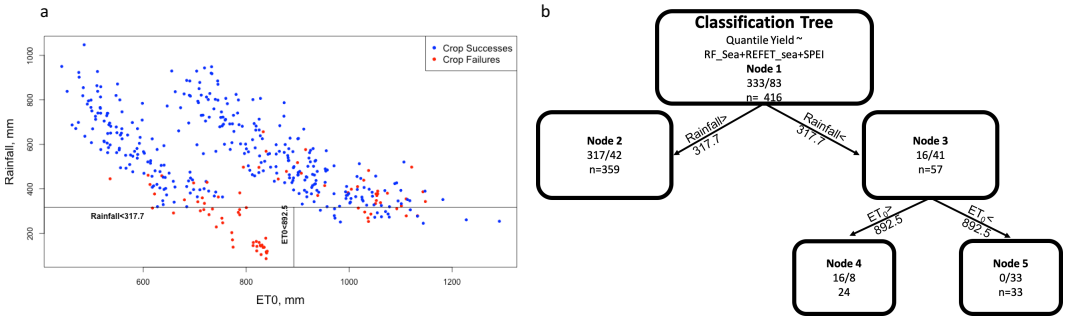

Figure 13. (**a**) The precipitation plotted against the ET_0, with the rules of the classification tree shown as lines. The first rule is precipitation is greater (less) than 317.7 mm, the next split is ET_0 is greater (less) than 892.5 mm. Crop failures are shown in red, and crop successes as defined by the 20th quantile are shown in blue. (**b**) the classification tree is shown, with 416 observations, 83 of which are crop failures. In Node 2, the precipitation is greater than 317.7 mm, with 317 of the 359 observations being crop successes (88%) and 42 of the observations being crop failures (12%). In Node 3, the observations have less than 317.7 mm of precipitation, resulting in 16 crop successes of the 57 observations (28%) and 41 crop failures (72%). Node 4 has ET_0 less than 892.5 mm, and of the 24 observations, 16 are crop successes (66.7%) and 8 are crop failures (33.3%). Finally, Node 5 has ET_0 less than 892.5 mm and has 33 observations, all of which are crop failures (100%)

4. Discussion

When constructing index insurance products, the choice of the dataset is extremely important, as the industry relies on stationary historical data to best match poor cropping years with payouts. Although this research did not investigate specific index designs, it is important to remember that even with data that is highly correlated to each other, small differences in design can lead to large differences with respect to product value [52]. The trends observed in ET_0 and precipitation were not similar throughout the season, and the structure of precipitation during the rainy season also changed

such that there were longer ends of the season and fewer dry pentads during the rainy season. Indices created for both datasets had radically different payout structures, and the agreement between the two indices was overall very low. The relationships between yield, precipitation, ET_0, and SPEI were relatively strong, with R-squared above 0.6 for all of these relationships. The classification trees and regression trees indicate that precipitation and ET_0 are useful in identifying poor yield years.

4.1. Precipitation Trends

The overall trends in the precipitation data are consistent with previous analysis of other datasets, specifically with an overall increase in precipitation in August, September, and October. However, there are few trends in the precipitation at the beginning of the rainy season, (Figure 2a,b). Consistent with our findings, ARC2 and GPCC precipitation datasets have positive increases for the whole rainy season in West Africa [53,54] and lower precipitation in the 1980s and increasing precipitation in the 1990s [54,55]. Although Biasutti [32] ran simulations of precipitation in the future with CMIP3 and CMIP5 [32], they find that by the year 2100, there would be significant changes across the Sahel in the beginning and end of the rainy season. Despite only analyzing data from the 1980s to the 2000s, we find a trend for the end of the season coming later, consistent with Biasutti [31,32].

The structure of the rainy season has also changed over time, with a decrease in the number of dry pentads and a delayed end of the season, as can be seen in Figure 3a. A later end of season date would be in accordance with Biasutti [31,32]. Additionally, fewer dry pentads indicate that the rainy season was more humid in the 1990s and 2000s, which would also be in accordance with L'Hôte [55] and Zhang [54].

4.2. ET_0 Trends

The ET_0 trends had no spatial pattern of the temporal trends. The decreases in ET_0 across the Sahel occur in August, consistent with other datasets [40], and the decreases in September are also consistent with other datasets [20]. The decrease in August ET_0 is consistent with a strengthening of the core of the rainy season in West Africa [56], where August receives more precipitation. An increase in precipitation during this month indicates increased cloud cover, and thus decreased evaporative demand. Although Cook et al. [20] found an overall increase of ET_0 during the early part of the rainy season in the Sahel, this analysis found no significant changes in ET_0 during the early part of the season.

Contrasting to the rest of West Africa, the Guinea Coast does have decreasing ET_0 for June, September, October, and the overall season, while July and August have either no trend or an increase directly over Cote d'Ivoire in August. The decreasing trend in June, September, October, and the overall season and absence thereof in July in August is an exception to the trend in the rest of West Africa. In a study that focused on the 1961–1990 period [57], the Guinea coast had the largest annual mean precipitation, cloud cover, and vapor pressure but the lowest mean temperature in West Africa. The ET_0 values along the coastlands are a reflection of the greater development of cloudiness in that zone, thereby reducing the incoming solar radiation with a consequent reflection in the net radiation available for ET_0 [57].

4.3. Precipitation and ET_0

Regressing ET_0 on precipitation, we find that increases in precipitation do lead to reductions in ET_0, most likely due to a reduction in incoming radiation due to increased cloud cover, as well as increased relative humidity. This relationship is particularly pronounced during August and appears to a lesser extent during September, October, and the season as a whole. Additionally, in September, October, and the overall season, large areas of West Africa have a negative relationship. June and July, however, have very little area with a significant relationship between ET_0 and precipitation.

While the long-term trends in ET_0 and precipitation are generally diverging, the spatial characterization of the trends are not especially tightly intertwined. August is the only month

that exhibits a coherent spatial signal between these two trends. For the Sahelian region of West Africa, there is a strong temperature–evapotranspiration relationship but a weak precipitation–evapotranspiration relationship [58]. As August is a month experiencing both an increase in precipitation and an increase in cloud cover resulting in a decrease in temperature, the resulting increase in precipitation across the 14–15th latitude corresponds with ET_0 decreasing. ET_0 is decreasing in September and precipitation is increasing as well, but the significant trend for ET_0 is concentrated in the westernmost part of West Africa.

4.4. Indices and Heidke Skill Score

The indices created for ET_0 and precipitation pay out differently for the majority of the rainy season. The payouts for precipitation occur mainly in the 1980s and early 1990s, especially during the months of August–October. The fact that the more payouts occur in the first half of the precipitation index confirms the previously established trend of increasing precipitation from the 1980s to present day. A majority of the payouts occurring in the first half of the dataset will result in farmers not getting enough payouts in the second half of the dataset. If precipitation were exclusively used for an index insurance product with data from 1981 to 2016, present-day farmers will likely experience too few payouts for it to be beneficial. However, ET_0 payouts occur mainly in the late 1990s to 2000s, with the exception of August.

ET_0 and precipitation have low agreement as measured with the Heidke Skill Score for most months except August. This divergence in payouts between precipitation and ET_0 indicates that these datasets may provide complementary information in capturing farming conditions during any given year. Considering the low number of payouts occurring in the 1999–2016 period for precipitation, ET_0 may well complement the precipitation data to cover poor cropping years in the second half of the dataset. Combining ET_0 and precipitation to create an index for insurance would be novel—but the concept of using multiple different datasets for indices is not. For example, index insurance in Ethiopia features a double trigger for insurance, where the early part of the season uses a precipitation index and the cessation of the season is evaluated with an Normalized Difference Vegetative Index (NDVI), a vegetation index [59]. In the case of Ethiopia, the addition of the vegetative index reduces the basis risk (the risk of the on-the-ground expectation not matching an index insurance payout) with the product.

4.5. Linear Fit of Yield with Precipitation, ET_0, and Spei

From the standpoint of plant physiology, in semiarid regions low crop yields should associate closely with precipitation, ET_0, and SPEI. Higher precipitation and SPEI should be associated with higher yields, and conversely, increased ET_0 should be associated with lower yields. Confirming these expected relationships, precipitation and SPEI both have positively significant slopes, while ET_0 has a negative significant slope, all with R-squared statistics above 0.60. A one-way analysis of variance (ANOVA) was conducted to compare the effect of precipitation/ET_0/SPEI and country on yield and showed that the effects were significant (results of these ANOVA tests are viewable in the Appendix A). An analysis of the yield data shows that three countries have positive trends over time, but the R-squared for these yields remain rather low and therefore do not explain a large amount of the variance. Additional information on the yield analysis can be found in the Appendix A.

An unexpected result from the model specification is that the best model had a fixed-slope across locations. The fixed-slope model is a less complex model than a freely varying model and has important practical implications: although regions are shifted relative to each other in terms of their ultimate crop yield potential, variation in yield is otherwise similarly responsive to a given environmental indicator.

4.6. Regression Tree

While the regression analysis is useful in confirming the hypothesized relationship between yield and the three regressors empirically, it does not inform whether the lowest outcomes on a regressor

align with the lowest yields, or whether the regressors may be combined to improve targeting the worst cropping years. Therefore, it is largely uninformative as the basis to improve index insurance. The regression model describes how the mean yield varies conditional on X, whereas our interest is in the left tail of the distribution, i.e., the low yields (A natural next step would then be to use quantile regression to model variation in the left tail of yield. We briefly pursued quantile regression but the results were not informative. In addition, the multicollinearity issue is present in using a blending of the three different covariates and is equally problematic for quantile regression and linear (conditional mean) regression). Further, the regression framework disallows use of the regressors in combination because they range from weakly to strongly collinear (as shown in Appendix A.2 Figure A3a–c).

The regression tree, viewable in Figure 9, finds that for many countries, low precipitation can reliably discriminate between high, medium, and low yields. Although the precise amount varies by country, precipitation determined low yield quantities for Burkina Faso, Mali, and Niger. However, using the ET_0 and precipitation in tandem was important for one country, Senegal. The first two rules for Senegal use ET_0 to separate the yield with a final rule using precipitation. SPEI was never used by the model to separate high and low yields. The classification and regression trees may not have used SPEI for any rules due to the fact that SPEI essentially duplicates information to the precipitation and ET_0.

4.7. Classification Tree

When using a classification tree, seen in Figure 13, to predict the discrete outcome category of lowest 20% of yield, the resulting tree was able to separate the data through precipitation and ET_0 into three nodes, two of which discriminated fairly well between crop failure (lowest 20%) and nonfailure (highest 80%). The resulting classification tree accurately showed that low yield has a relationship to low precipitation and high ET_0. SPEI was not used in separating out the different outcomes of yield.

5. Conclusions

Precipitation-based indices are useful for identifying probable poor yield seasons, particularly in water limited areas like in the Sahel. However, historical precipitation trends can substantially impact a payout schedule, and designers of insurance indices need to account for these trends. Since index insurance is a relatively new risk management strategy, there is limited exploration for solutions to trends in datasets. Many groups have identified trends in data as a problem, particularly when it comes to climate change impacts [11,60]. Some have suggested that insurers incorporate the uncertainty due to trends in the price of index insurance [61], but this may result in index insurance becoming too expensive for farmers to afford. Other possible solutions could be to incorporate seasonal forecasts, decadal trends, or climate change into index insurance contracts [11].

If payout models are to be built using only a single predictor among precipitation, ET_0 and SPEI, this work indicates that any of these datasets are equally useful in creating an index. In fact, the datasets could be interchangeable depending on the preferences of the farmers and the insurance company. Surprisingly, there are no great gains in using SPEI instead of precipitation and ET_0. Due to these results being so similar, it might make sense in the near-term to continue using precipitation for indices. Precipitation is relatively understandable: if a specific level of precipitation is not achieved, there is a payout, otherwise there is no payout. However, as the trends between precipitation and ET_0 are not the same, it would be prudent to continue to monitor the relationships between ET_0 and SPEI to yield.

Conversely, we present evidence supporting the use of multiple datasets when making index insurance contracts in the future. The precipitation works fairly well as a first rule to understand poor yields, but ET_0 is used in the classification tree to determine the worst yields. On a theoretical basis, SPEI may actually be a useful indicator for yield in the future. It performs equally well to precipitation and ET_0 in regressions currently, although it is not used for any rules in the classification or regression trees. For the time being, precipitation and ET_0 perform well in indicating low and high yield results, but as climate change impacts temperatures [39] and natural climate variability impacts

precipitation [23,30,40,55,62,63], SPEI might be the best way to ensure that poor cropping years are covered for farmers.

Although not included in the scope of this paper, combinations of datasets may better capture crop losses experienced by farmers. For example, considering the relatively low Heidke Skill Score of ET_0 and precipitation payouts, a combined index would capture different bad years, potentially to the benefit of the farmers. An indicator not investigated in this paper is NDVI, which has shown promise for potential use in index insurance in West Africa [12] and is already used in other regions for index insurance [64]. Traditionally, there are few indices that use NDVI in West Africa, with precipitation and ET_0 preferred for index design, which is the basis of the research in this analysis. However, NDVI has been proven to accurately indicate drought conditions in other parts of the world [65]. There is evidence that in Sahalian West Africa, vegetation is driven by precipitation and that NDVI can be used to assess changes in crop production [66]. One potential avenue for future research is multiple trigger index insurance for West Africa, such as in Ethiopia, where NDVI is used as a complementary trigger for detecting drought alongside precipitation [49,59], or using NDVI as a stand-alone indicator for index insurance [12], given it has proper calibration [67].

Index design and data processing can greatly affect the quality of the final insurance product; this aspect is crucial to ensuring that smallholder farmers get the best option for an insurance product. Meroni 2019 [68] produced estimates of near real time NDVI anomalies by consolidating new incoming data with prior information smoothing and updating the estimates as new data became available to more accurately capture crop health quickly. As the precipitation and ET_0 datasets are available at different temporal scales, similar innovative methods to integrate data at different temporal scales will be necessary to create. As was highlighted in this study, precipitation and ET_0 do not exhibit similar trends, which could represent an opportunity to capture information pertinent to improving the poor cropping years.

Future research should investigate how ET_0 is affected by its different drivers, in order to have a better understanding of the spatial variation in the trends as observed in this paper. Although precipitation is relatively well understood, more research on extreme rainfall events could lead to options in coverage for affected farmers. Ultimately, ET_0 and precipitation both have trends in their datasets, which impact the identification of payout years. These two datasets capture complementary aspects of water shortages, one capturing the deficit of water input to the system while the other captures enhancement of the water needed by the system. Innovative approaches utilizing the combination of these two dynamics should result in financial instruments which better serve farmers in the developing world by helping them mitigate the impacts of drought events.

Author Contributions: The authors contributed to this work in the following ways: Conceptualization, S.L.B., S.S., G.H., L.H., C.F. and D.E.O.; Data curation, P.P.; Formal analysis, S.L.B., S.S., G.H. and C.F.; Funding acquisition, G.H. and C.F.; Investigation, S.L.B.; Methodology, S.L.B., S.S., G.H. and C.F.; Project administration, G.H.; Resources, G.H. and C.F.; Software, P.P.; Supervision, G.H.; Validation, S.L.B. and S.S.; Visualization, S.L.B.; Writing—original draft, S.L.B., S.S., G.H. and C.F.; Writing—review and editing, S.L.B., S.S., G.H., L.H., C.F. and D.E.O. All authors have read and agreed to the published version of the manuscript.

Funding: This work was supported by NASA project NNX14AD64G, USGS Cooperative Agreement Number G14AC00042, United States Agency for International Development Cooperative Agreement 72DFFP19CA00001, and the USGS Drivers of Drought Program funded Chris Funk.

Acknowledgments: Susan Meerdink, Rafael Guimarães Ramos, Catherine Pomposi, James Allen, David L Miller, Lauren Smyth, and Sophia Arabadjis.

Conflicts of Interest: The authors declare no conflict of interest. The funders had no role in the design of the study; in the collection, analyses, or interpretation of data; in the writing of the manuscript, or in the decision to publish the results.

Appendix A

Appendix A.1. Standard Deviation and Coefficient of Variation for Precipitation and ET_0

An analysis of the variability, through standard deviation, averages, and coefficient of variation was conducted to better understand the relevant magnitudes of variability within both the precipitation

and ET_0.Consistent with the findings of Husak 2018 [69], the standard deviation of precipitation (Figure A1) is always greater than that of ET_0 (Figure A2). However, comparing the standard deviations for both variables can be misleading since the means of each dataset are both different and vary across space, (Figure A1g-l and Figure A2g–l). The coefficient of variation expresses the variability in relation to the mean, thereby allowing for a direct comparison between the precipitation and the ET_0. Comparing the coefficients of variability between ET_0 in Figure A2m–r and precipitation in Figure A2m–r, it is clear that precipitation has a higher range of variability. For all months, the coefficient of variability for precipitation is larger than the coefficient of variability for ET_0. From comparing the coefficients of variability, it is clear that the SPEI data would vary more due to the precipitation dataset as opposed to the ET_0.

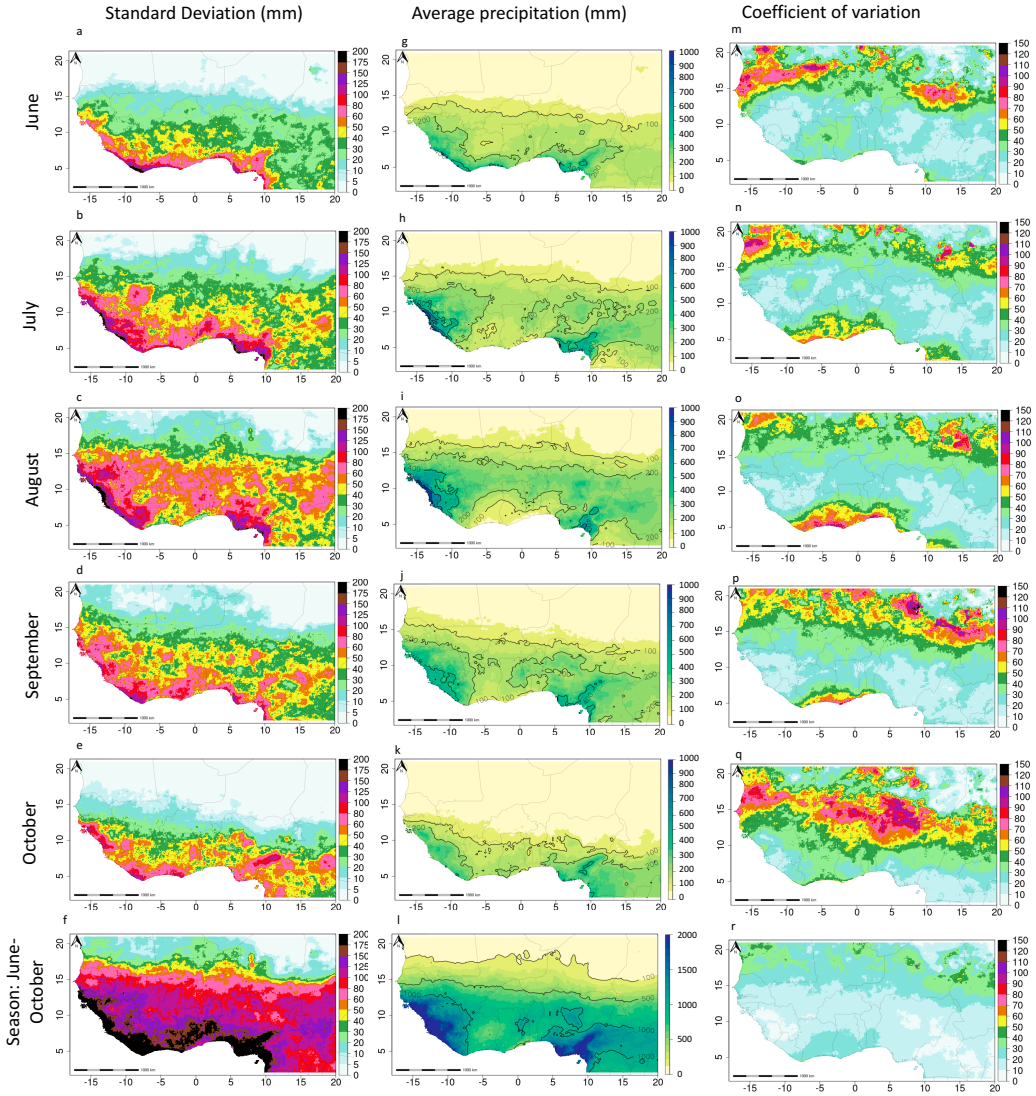

Figure A1. These three columns show the variability for precipitation from 1981 to 2016. The right-hand column (**a**–**f**) has the standard deviation by month expressed in mm/month (mm/season for (**f**), June (**a**), July (**b**), August (**c**), September (**d**), October (**e**), and the whole season (**f**) for 1981–2016. The middle column (**g**–**l**)shows the average precipitation per month (expressed in mm/month or mm/season for (**l**)) for June (**g**), July (**h**), August (**i**), September (**j**), October (**k**), and the whole season (**l**). The left-hand column (**m**–**r**) has the coefficient of variation per month expressed in percentage for June (**m**), July (**n**), August (**o**), September (**p**), October (**q**), and the whole year (**r**).

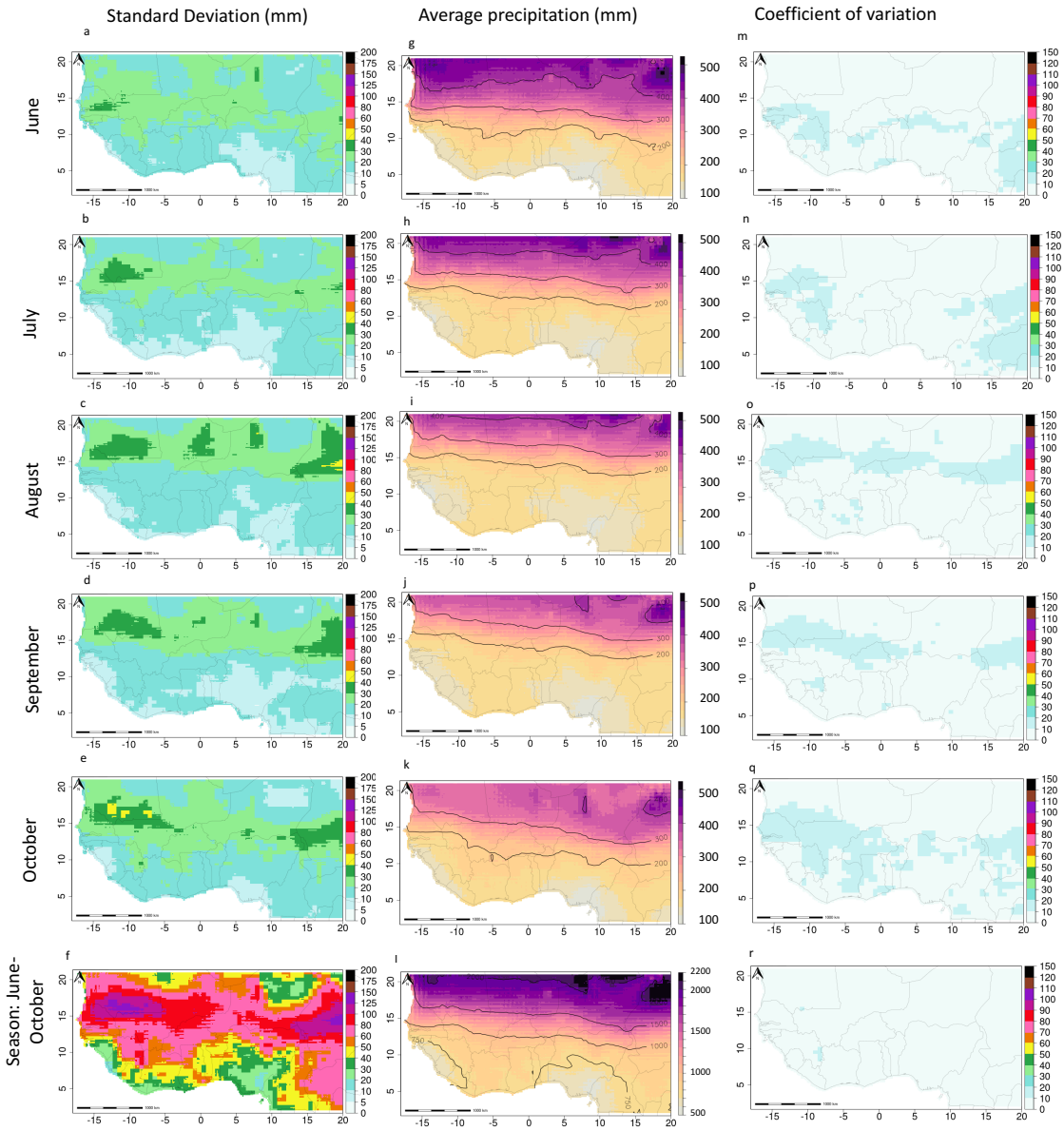

Figure A2. These three columns show the variability for ET_0 from 1981 to 2016. The right-hand column (**a**–**f**) has the standard deviation by month as expressed in mm/month (seasonal is mm/season), June (**a**), July (**b**), August (**c**), September (**d**), October (**e**), and the whole season (**f**) for 1981–2016. The middle column (**g**–**l**)shows the average ET_0 per month (expressed in mm/month or mm/season for **l** for June (**g**), July (**h**), August (**i**), September (**j**), October (**k**), and the whole season (**l**). The left-hand column (**m**–**r**) has the coefficient of variation per month expressed in percentages for June (**m**), July (**n**), August (**o**), September (**p**), October (**q**), and the whole year (**r**).

Appendix A.2. ET_0 Precipitation and Spei Relationships

Before comparing ET_0, precipitation, and SPEI to yield, these agroclimatic indicators were compared to each other. As expected, the relationship between ET_0 and precipitation is negative (see Figure A3a). The SPEI is positively associated with precipitation, although the relationship is weak (see Figure A3c) whereas there is almost no association between ET_0 and SPEI (see Figure A3b).

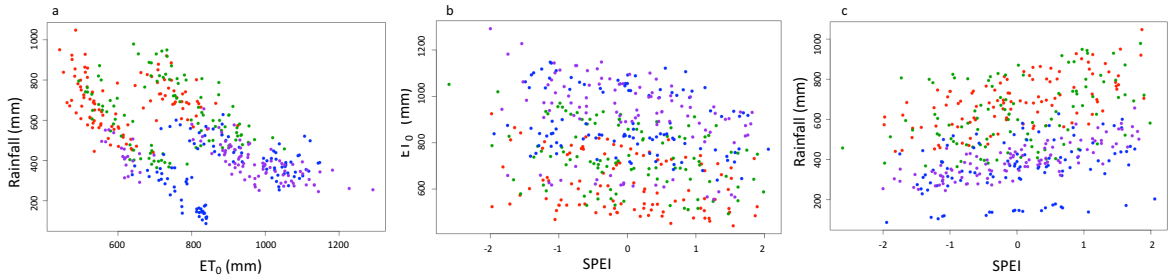

Figure A3. (**a**) The relationship between precipitation and ET_0. (**b**) The relationship between precipitation and SPEI. (**c**) The relationship between ET_0 and SPEI. The regions are identified by the colors in each plot, with red indicating Burkina Faso, green is Mali, blue indicating Niger, and purple indicating Senegal.

Appendix A.3. Specification Testing for Yield Regressions

There are three potential model parameterizations to assess the effects of country, yield, and an environmental indicator (precipitation, SPEI, reference evapotranspiration). The least constrained of these models is a random effects model where, seen in (A1), both the intercept and estimate of effects of the environmental indicator are allowed to vary across time and location (region). On the other hand, the most constrained model would be (A3), where both the intercept and slope are constrained. This "null" model reflects no time variance or region variance, and is simply an estimate of overall means across West Africa. It is not useful for this analysis. Between these two models, there are two possible constraints we could use, one to constrain the slope and allow the intercept to vary and one to constrain the intercept and allow the slope to vary. Both of these models are inherently more relevant to this research, and we tried both specifications. The final model is a compromise between the most constrained model (A3) and the least constrained model (A1), where the intercept varies but the slope does not, seen in (A2).

$$y_{i,t} = \alpha_i + \beta_{1,i} X_{i,t} + u_{i,t} \tag{A1}$$

where $y_{i,t}$ is the region (i) and year (t) indexed yield, and $X_{i,t}$ is either precipitation, ET_0, or SPEI. The coefficient estimates returned from (A1) are identical to those derived from separate country-specific regressions. Specification testing, using F-tests and AIC, can be used to evaluate whether restricted versions of (A1) are superior in terms of providing as good or better fit to the data but using fewer parameters. One option is to use a common slope term with varying intercepts:

$$y_{i,t} = \alpha_i + \beta_1 X_{i,t} + u_{i,t} \tag{A2}$$

the other option is to use varying slopes with fixed intercept:

$$y_{i,t} = \alpha + \beta_1 X_{i,t} + u_{i,t} \tag{A3}$$

Specification testing indicates that the fixed slope, varying intercept model (A2) is the best. The F-tests and AIC results can be found in Table A1.

F-Test

Table A1. Different *p*-values are used to determine significance. *** represent estimates that have *p*-values smaller than 0.001.

Precipitation	Degrees of Freedom	Sum of Squares	F-statistic	Pr(>F)
Model 1, Model 2	19	7.45	12.85	$<2.2 \times 10^{-16}$ ***
Model 2, Model 3	19	0.77	1.34	0.15
Model 1, Model 3	38	8.21	7.21	2.2×10^{-16} ***
ET_0	**Degrees of Freedom**	**Sum of Squares**	**F-statistic**	**Pr(>F)**
Model 1, Model 2	19	21.44	36.71	$<2.2 \times 10^{-16}$ ***
Model 2, Model 3	19	0.53	0.90	0.58
Model 1, Model 3	38	8.21	7.21	2.2×10^{-16} ***
SPEI	**Degrees of Freedom**	**Sum of Squares**	**F-statistic**	**Pr(>F)**
Model 1, Model 2	19	25.28	44.21	$<2.2 \times 10^{-16}$ ***
Model 2, Model 3	19	0.56	0.97	0.49
Model 1, Model 3	38	25.83	22.53	$<2.2 \times 10^{-16}$ ***

Appendix A.4. Yield Analysis

Looking at the plots of yield over time in Figure A4, the yield for all locations has a relatively low R-squared, with only one country, Niger, having an R-squared that is relatively large, at 0.17 (all the rest are below 0.10). The slopes for Burkina Faso, Niger, and Senegal are all significant, with the slope for Mali's yield remaining insignificant.

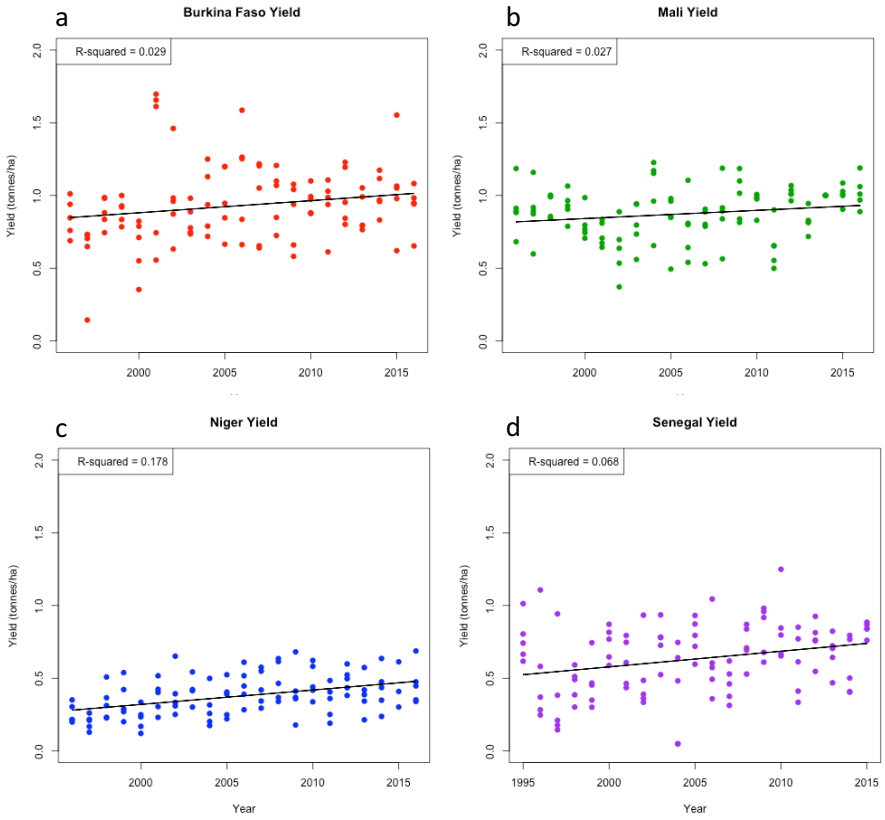

Figure A4. Yield (tonnes/ha) plotted against time for (**a**) Burkina Faso, (**b**) Mali, (**c**) Niger, and (**d**) Senegal.

Yield Regressions

Table A2. Numbers within the brackets () represent the standard error of the estimate directly above themselves. Different *p*-values are used to determine significance—* represents estimates that *p*-values smaller than 0.05, and *** represent estimates that have *p*-values smaller than 0.001.

Burkina Faso		
	Estimate	**pr(>t)**
Intercept	−15.74	0.057
	(8.19)	
Slope	0.008	0.044 *
	(0.004)	
Adjusted R-squared		0.029
F-statistic		4.15
p-value		0.04
Mali		
	Estimate	**pr(>t)**
Intercept	−10.41	0.072
	(5.72)	
Slope	0.006	0.051
	(0.003)	
Adjusted R-squared		0.027
F-statistic		3.89
p-value		0.051
Niger		
	Estimate	**pr(>t)**
Intercept	−19.5	8.55×10^{-5} ***
	(4.15)	
Slope	0.01	5.93e-6 ***
	(0.002	
Adjusted R-squared		0.178
F-statistic		22.89
p-value		5.93×10^{-6}
Senegal		
	Estimate	**pr(>t)**
Intercept	−20.94	5.00×10^{-3} ***
	(7.37)	
Slope	0.011	4.00×10^{-3} ***
	(0.004)	
Adjusted R-squared		0.068
F-statistic		8.58
p-value		4.00×10^{-3}

Appendix A.5. One-Way Anova Results for Linear Fit for Yield with Precipitation, ET_0, and Spei

An Analysis of Variance (ANOVA) compares the sum of squares for each variable against the sum of squares for the residuals and uses these metrics to construct the F-statistic. The F-statistic is used to determine if the explanatory variable does not improve the prediction of the dependent variable from the average of the dependent variable (null hypothesis), or in other words, randomness explains the dependent variable better than the regression model. In our case, the F-statistic is larger than the critical F-statistic, and the *p*-value for the F-statistic is small for precipitation, ET_0, and SPEI. This indicates that for all three models, an intercept alone does not explain the majority of the variance

in the model, rather that the slopes for these models are significantly contributing to the improvement of the model.

Appendix A.5.1. One-Way ANOVA Precipitation

Table A3. *** represent estimates that have *p*-values smaller than 0.001.

	Degrees of Freedom	Sum of Squares	Mean Square	*F*-Value	Pr(F)
Precipitation	1	18.26	18.26	599	$<2.2 \times 10^{-16}$ ***
Country	19	7.45	0.39	12.9	$<2.2 \times 10^{-16}$ ***
Residuals	395	12.04	0.03		

Appendix A.5.2. One-Way ANOVA ET_0

Table A4. *** represent estimates that have *p*-values smaller than 0.001.

	Degrees of Freedom	Sum of Squares	Mean Square	*F*-Value	Pr(F)
ET_0	1	4.17	4.17	135.54	$<2.2 \times 10^{-16}$ ***
Country	19	21.44	1.13	36.71	$<2.2 \times 10^{-16}$ ***
Residuals	395	12.14	0.03		

Appendix A.5.3. One-Way ANOVA SPEI

Table A5. *** represent estimates that have *p*-values smaller than 0.001.

	Degrees of Freedom	Sum of Squares	Mean Square	*F*-Value	Pr(F)
ET_0	1	0.59	0.59	19.53	$<1.28 \times 10^{-5}$ ***
Country	19	25.28	1.33	44.21	$<2.2 \times 10^{-16}$ ***
Residuals	395	11.89	0.03		

References

1. Cole, S.; Giné, X.; Tobacman, J.; Topalova, P.; Townsend, R.; Vickery, J. Barriers to household risk management: Evidence from India. *Am. Econ. J. Appl. Econ.* **2013**, *5*, 104–135. [CrossRef]
2. Marteau, R.; Sultan, B.; Moron, V.; Alhassane, A.; Baron, C.; Traoré, S.B. The onset of the rainy season and farmers' sowing strategy for pearl millet cultivation in Southwest Niger. *Agric. For. Meteorol.* **2011**, *151*, 1356–1369. [CrossRef]
3. Barrett, C. Covariate Catastropic Risk Management in the Developing World: Discussion. *Am. J. Agric. Econ.* **2011**, *93*, 512–513. [CrossRef]
4. *Regional Overview of Food Insecurity Africa: African Food Security Prospects Brighter than Ever*; Technical Report; FAO: Rome, Italy, 2015.
5. Barrett, C.B.; Barnett, B.J.; Carter, M.R.; Chantarat, S.; Hansen, J.W.; Mude, A.G.; Osgood, D.; Skees, J.R.; Turvey, C.G.; Ward, M.N. *Poverty Traps and Climate Risk: Limitations and Opportunities of Index-Based Risk Financing*; International Research Institute for Climate and Society: New York, NY, USA, 2007.
6. Matlon, P.J. Farmer risk management strategies: The case of the West African semi-arid tropics. In *Risk in Agriculrure: Proceeding of the Tenth Agriculture Sector Symposium*; The World Bank: Washington, DC, USA, 1991.
7. Lin, B.B. Resilience in agriculture through crop diversification: adaptive management for environmental change. *BioScience* **2011**, *61*, 183–193. [CrossRef]
8. Xoconostle-Cázares, B.; Ramirez-Ortega, F.A.; Flores-Elenes, L.; Ruiz-Medrano, R. Drought tolerance in crop plants. *Am. J. Plant. Physiol.* **2010**, *5*, 1–16.
9. Evenson, R.E.; Gollin, D. Assessing the impact of the Green Revolution, 1960 to 2000. *Science* **2003**, *300*, 758–762. [CrossRef]

10. Vohland, K.; Barry, B. A review of in situ rainwater harvesting (RWH) practices modifying landscape functions in African drylands. *Agric. Ecosyst. Environ.* **2009**, *131*, 119–127. [CrossRef]
11. Hellmuth, M.; Osgood, D.; Hess, U.; Moorhead, A.; Bhojwani, H. *Index insurance and Climate Risk: Prospoects for Development and Disaster Management*; Climate and Society No. 2; WCAS: New York, NY, USA, 2009.
12. *Remote Sensing for Index Insurance, An Overview of Findings and Lessons Learned for Smallholder Agriculture, Report*; Technical Report; International Fund of Agricultural Development: Rome, Italy, 2017.
13. Madajewicz, M.; Tsegay, H.; Norton, M. *Managing Risks to Agricultural Livelihoods: Impact Evaluation of the Harita Progam in Tigray, 2009–2012*; Oxfam: Boston, MA, USA, 2013.
14. Funk, C.C.; Brown, M.E. Declining global per capita agricultural production and warming oceans threaten food security. *Food Secur.* **2009**, *1*, 271–289. [CrossRef]
15. R4 Rural Resilience Initiative, Annual Report: January–December 2018. Technical Report, World Food Programme. 2018. Available online: https://docs.wfp.org/api/documents/WFP-0000104178/download/ (accessed on 28 April 2020).
16. *PlaNet Guarantee: Benin, Burkina Faso, Mali, Senegal. Global Index Insurance Facility (GIIF) Partner Profile*; Technical Report; World Bank: Washington, DC, USA, 2017; (In English). Available online: http://documents.worldbank.org/curated/en/787441490703399516/PlaNet-guarantee-Benin-Burkina-Faso-Mali-Senegal (accessed on 28 April 2020).
17. *Assurance Agricole Basee sur un Indice Climatique au Senegal*; Technical Report; Global Index Insurance Fund (GIIF), World Bank Group: Washington, DC, USA, 2018. Available online: https://www.indexinsuranceforum.org/sites/default/files/19677_SenegalConference_4pager_FRE_final_%20March%2018.pdf (accessed on 28 April 2020).
18. *African Risk Capacity Funds Assisted at Least 2.1 Million People Affected by Drought*; Technical Report; African Risk Capacity: Rome, Italy, 2018. Available online: https://www.africanriskcapacity.org/wp-content/uploads/2018/05/Payouts-and-Successes_2018_EN.pdf (accessed on 28 April 2020).
19. Coleman, E.; Dick, W.; Gilliams, S.; Piccard, I.; Rispoli, F.; Stoppa, A. *Remote Sensing for Index Insurance, Findings and Lessons Learned for Smallholder Agriculture*; Technical Report; International Fund of Agricultural Development (IFAD): Rome, Italy, 2018. Available online: https://www.ifad.org/documents/38714170/39144386/RemoteSensing_LongGuide_2017.pdf/f2d22adb-c3b0-4fe3-9cbb-c25054d756fe (accessed on 28 April 2020).
20. Cook, K.H.; Vizy, E.K. Impact of climate change on mid-twenty-first century growing seasons in Africa. *Clim. Dyn.* **2012**, *39*, 2937–2955. [CrossRef]
21. Cornforth, R. Overview of the West African monsoon 2011. *Weather* **2012**, *67*, 59–65. [CrossRef]
22. Nicholson, S.E.; Some, B.; Kone, B. An analysis of recent rainfall conditions in West Africa, including the rainy seasons of the 1997 El Niño and the 1998 La Niña years. *J. Clim.* **2000**, *13*, 2628–2640. [CrossRef]
23. Nicholson, S. On the question of the recovery of the rains in the West African Sahel. *J. Arid. Environ.* **2005**, *63*, 615–641. [CrossRef]
24. Nicholson, S.E. The West African Sahel: A review of recent studies on the rainfall regime and its interannual variability. *Isrn Meteorol.* **2013**, *2013*, 453521. [CrossRef]
25. Hayward, D.; Oguntoyinbo, J.S. *Climatology of West Africa*; Science: London, UK, 1987.
26. Funk, C.; Peterson, P.; Landsfeld, M.; Pedreros, D.; Verdin, J.; Shukla, S.; Husak, G.; Rowland, J.; Harrison, L.; Hoell, A.; et al. The climate hazards infrared precipitation with stations—A new environmental record for monitoring extremes. *Sci. Data* **2015**, *2*, 1–21. [CrossRef] [PubMed]
27. Hobbins, M.; Harrison, L.; Blakeley, S.L.; Dewes, C.; Husak, G.J.; Shukla, S.; Jayanthi, H.; McNally, A.; Sarmiento, D.; Verdin, J. Drought in Africa: Understanding and Exploiting the Demand Perspective Using a New Evaporative Demand Reanalysis. *AGUFM* **2018**, *2018*, GC21D-1121.
28. Hobbins, M.; Dewes, C.; Jayanthi, H.; McNally, A.; Sarmiento, D.; Shukla, S.; Verdin, J. Developing and exploiting a new global reanalysis of evaporative demand for global food-security assessments and drought monitoring. In Proceedings of the American Meteorological Society Annual Meeting, Phoenix, AZ, USA, 6–10 January 2019.
29. Rodrigues, L.R.L.; García-Serrano, J.; Doblas-Reyes, F. Seasonal forecast quality of the West African monsoon rainfall regimes by multiple forecast systems. *J. Geophys. Res. Atmos.* **2014**, *119*, 7908–7930. [CrossRef]
30. Giannini, A.; Saravanan, R.; Chang, P. Oceanic forcing of Sahel rainfall on interannual to interdecadal time scales. *Science* **2003**, *302*, 1027–1030. [CrossRef]

31. Biasutti, M.; Sobel, A.H. Delayed Sahel rainfall and global seasonal cycle in a warmer climate. *Geophys. Res. Lett.* **2009**, *36*, 23. [CrossRef]
32. Biasutti, M. Forced Sahel rainfall trends in the CMIP5 archive. *J. Geophys. Res. Atmos.* **2013**, *118*, 1613–1623. [CrossRef]
33. Allen, R.G.; Pereira, L.S.; Raes, D.; Smith, M. *Crop evapotranspiration-Guidelines for Computing Crop Water Requirements*; FAO Irrigation and Drainage Paper 56; FAO: Rome, Italy, 1998; Volume 300, p. D05109.
34. Hobbins, M.T.; Wood, A.; McEvoy, D.J.; Huntington, J.L.; Morton, C.; Anderson, M.; Hain, C. The evaporative demand drought index. Part I: Linking drought evolution to variations in evaporative demand. *J. Hydrometeorol.* **2016**, *17*, 1745–1761. [CrossRef]
35. Peng, L.; Li, Y.; Feng, H. The best alternative for estimating reference crop evapotranspiration in different sub-regions of mainland China. *Sci. Rep.* **2017**, *7*, 5458. [CrossRef] [PubMed]
36. Sultan, B.; Roudier, P.; Quirion, P.; Alhassane, A.; Muller, B.; Dingkuhn, M.; Ciais, P.; Guimberteau, M.; Traore, S.; Baron, C. Assessing climate change impacts on sorghum and millet yields in the Sudanian and Sahelian savannas of West Africa. *Environ. Res. Lett.* **2013**, *8*, 014040. [CrossRef]
37. Prasad, P.; Staggenborg, S.; Ristic, Z. Impacts of drought and/or heat stress on physiological, developmental, growth, and yield processes of crop plants. In *Response of Crops to Limited Water: Understanding and Modeling Water Stress Effects on Plant Growth Processes*; American Society of Agronomy: Madison, WI, USA, 2008; pp. 301–355.
38. Wheeler, T.R.; Craufurd, P.Q.; Ellis, R.H.; Porter, J.R.; Prasad, P.V. Temperature variability and the yield of annual crops. *Agric. Ecosyst. Environ.* **2000**, *82*, 159–167. [CrossRef]
39. Field, C.B. *Climate Change 2014—Impacts, Adaptation and Vulnerability: Regional Aspects*; Cambridge University Press: Cambridge, UK, 2014.
40. Estes, L.D.; Chaney, N.W.; Herrera-Estrada, J.; Sheffield, J.; Caylor, K.K.; Wood, E.F. Changing water availability during the African maize-growing season, 1979–2010. *Environ. Res. Lett.* **2014**, *9*, 075005. [CrossRef]
41. *R4 Rural Resilience Initiative: Quarterly Report, July–September 2016*; Technical Report; World Food Programme: Rome, Italy, 2016.
42. Svoboda, M.; Fuchs, B. *Handbook of Drought Indicators and Indices*; *Integrated Drought Management Tools and Guidelines Series 2, Geneva*; World Meteorological Organization and Global Water Partnership, Geneva, Switzerland, 2016.
43. Hobbins, M.; McNally, A.; Sarmiento, D.; Jansma, T.; Husak, G.; Turner, W.; Verdin, J. Using a New Evaporative Demand Reanalysis to Understand the Demand Perspective of Drought and Food Insecurity in Africa. In Proceedings of the 100th American Meteorological Society Annual Meeting, Boston, MA, USA, 12–16 January 2020.
44. Hobbins, M.; McNally, A.; Sarmiento, D.; Verdin, J. Drought in Africa: Understanding and Exploiting the Demand Perspective Using A New Evaporative Demand Reanalysis. In Proceedings of the European Meteorological Society Annual Meeting, Copenhagen, Denmark, 9–13 September 2019.
45. Allen, R.G.; Clemmens, A.J.; Burt, C.M.; Solomon, K.; O'Halloran, T. Prediction accuracy for projectwide evapotranspiration using crop coefficients and reference evapotranspiration. *J. Irrig. Drain. Eng.* **2005**, *131*, 24–36. [CrossRef]
46. Gelaro, R.; McCarty, W.; Suárez, M.J.; Todling, R.; Molod, A.; Takacs, L.; Randles, C.A.; Darmenov, A.; Bosilovich, M.G.; Reichle, R.; et al. The modern-era retrospective analysis for research and applications, version 2 (MERRA-2). *J. Clim.* **2017**, *30*, 5419–5454. [CrossRef]
47. Vicente-Serrano, S.M.; Beguería, S.; López-Moreno, J.I.; Angulo, M.; El Kenawy, A. A new global 0.5 gridded dataset (1901–2006) of a multiscalar drought index: Comparison with current drought index datasets based on the Palmer Drought Severity Index. *J. Hydrometeorol.* **2010**, *11*, 1033–1043. [CrossRef]
48. Vicente-Serrano, S.M.; Beguería, S.; López-Moreno, J.I. A multiscalar drought index sensitive to global warming: the standardized precipitation evapotranspiration index. *J. Clim.* **2010**, *23*, 1696–1718. [CrossRef]
49. De Leeuw, J.; Vrieling, A.; Shee, A.; Atzberger, C.; Hadgu, K.M.; Biradar, C.M.; Keah, H.; Turvey, C. The potential and uptake of remote sensing in insurance: A review. *Remote Sens.* **2014**, *6*, 10888–10912. [CrossRef]

50. Norton, M.; Osgood, D.; Madajewicz, M.; Holthaus, E.; Peterson, N.; Diro, R.; Mullally, C.; Teh, T.L.; Gebremichael, M. Evidence of demand for index insurance: Experimental games and commercial transactions in Ethiopia. *J. Dev. Stud.* **2014**, *50*, 630–648. [CrossRef]
51. Barnston, A.G. Correspondence among the correlation, RMSE, and Heidke forecast verification measures, refinement of the Heidke score. *Weather Forecast.* **1992**, *7*, 699–709. [CrossRef]
52. Jensen, N.; Stoeffler, Q.; Fava, F.; Vrieling, A.; Atzberger, C.; Meroni, M.; Mude, A.; Carter, M. Does the design matter? Comparing satellite-based indices for insuring pastoralists against drought. *Ecol. Econ.* **2019**, *162*, 59–73. [CrossRef]
53. Wang, G.; Alo, C.A. Changes in precipitation seasonality in West Africa predicted by RegCM3 and the impact of dynamic vegetation feedback. *Int. J. Geophys.* **2012**, *2012*, 597205. [CrossRef]
54. Zhang, W.; Brandt, M.; Guichard, F.; Tian, Q.; Fensholt, R. Using long-term daily satellite based rainfall data (1983–2015) to analyze spatio-temporal changes in the sahelian rainfall regime. *J. Hydrol.* **2017**, *550*, 427–440. [CrossRef]
55. L'HOTE, Y.; Mahe, G.; Some, B. The 1990s rainfall in the Sahel: the third driest decade since the beginning of the century. *Hydrol. Sci. J.* **2003**, *48*, 493–496. [CrossRef]
56. Nicholson, S.E.; Funk, C.; Fink, A.H. Rainfall over the African continent from the 19th through the 21st century. *Glob. Planet. Chang.* **2018**, *165*, 114–127. [CrossRef]
57. Abiye, O.E.; Matthew, O.J.; Sunmonu, L.A.; Babatunde, O.A. Potential evapotranspiration trends in West Africa from 1906 to 2015. *Appl. Sci.* **2019**, *1*, 1434. [CrossRef]
58. Marshall, M.; Funk, C.; Michaelsen, J. Examining evapotranspiration trends in Africa. *Clim. Dyn.* **2012**, *38*, 1849–1865. [CrossRef]
59. *R4 Rural Resilience Initiative Annual Report January–December 2018*; Technical Report; World Food Programme: Rome, Italy, 2018.
60. Collier, B.; Skees, J.; Barnett, B. Weather index insurance and climate change: opportunities and challenges in lower income countries. *Geneva Pap. Risk Insur. Issues Pract.* **2009**, *34*, 401–424. [CrossRef]
61. Shirley, K.; Osgood, D.; Robert, A.; Block, P.; Lall, U.; Hansen, J.; Kirshener, S.; Moron, V.; Ines, A.; TUrvey, C.; et al. Rainfall Modeling and Simulation. Paper Presented at a workshop on 'Technical Issues in Index Insurance, IRI, Columbia University, New York, NY, USA, 7–8 October 2008. Available online: http://iri.columbia.edu/csp/issue2/workshop (accessed on 28 April 2020).
62. Hoerling, M.; Hurrell, J.; Eischeid, J.; Phillips, A. Detection and attribution of twentieth-century northern and southern African rainfall change. *J. Clim.* **2006**, *19*, 3989–4008. [CrossRef]
63. Zhang, R.; Delworth, T.L.; Sutton, R.; Hodson, D.L.; Dixon, K.W.; Held, I.M.; Kushnir, Y.; Marshall, J.; Ming, Y.; Msadek, R.; et al. Have aerosols caused the observed Atlantic multidecadal variability? *J. Atmos. Sci.* **2013**, *70*, 1135–1144. [CrossRef]
64. Chantarat, S.; Mude, A.G.; Barrett, C.B.; Carter, M.R. Designing index-based livestock insurance for managing asset risk in northern Kenya. *J. Risk Insur.* **2013**, *80*, 205–237. [CrossRef]
65. Klisch, A.; Atzberger, C. Operational drought monitoring in Kenya using MODIS NDVI time series. *Remote Sens.* **2016**, *8*, 267. [CrossRef]
66. Louise, L.; Agnès, B.; Danny, L.S. Regional analysis of crop and natural vegetation in West Africa based on NDVI metrics. In Proceedings of the 2014 IEEE Geoscience and Remote Sensing Symposium, Quebec City, QC, Canada, 13–18 July 2014; pp. 5107–5110.
67. Turvey, C.G.; Mclaurin, M.K. Applicability of the normalized difference vegetation index (NDVI) in index-based crop insurance design. *Weather. Clim. Soc.* **2012**, *4*, 271–284. [CrossRef]
68. Meroni, M.; Fasbender, D.; Rembold, F.; Atzberger, C.; Klisch, A. Near real-time vegetation anomaly detection with MODIS NDVI: Timeliness vs. accuracy and effect of anomaly computation options. *Remote Sens. Environ.* **2019**, *221*, 508–521. [CrossRef]
69. Husak, G.; Shukla, S.; Funk, C.; Hobbins, M. Investigating the Inputs to SPEI and Their Importance in Identifying Agroclimatic Hazards. In Proceedings of the AGU Fall Meeting Abstracts, Washington, DC, USA, 10–14 December 2018.